

Complete one-loop QED corrections to D_s^+ leptonic decays and impact on the CKM unitarity test

Teppei Kitahara^{a,b}, Jun Miyamoto^{c,a} and Kota Sasaki^{d,a}

^a*Department of Physics, Graduate School of Science, Chiba University, Chiba 263-8522, Japan*

^b*Kobayashi-Maskawa Institute for the Origin of Particles and the Universe, Nagoya University, Furo-cho Chikusa-ku, Nagoya 464-8602 Japan*

^c*ICRR, The University of Tokyo, Kashiwa, Chiba 277-8582, Japan*

^d*Department of Physics, Graduate School of Science and Engineering, Chiba University, 263-8522, Chiba, Japan*

E-mail: kitahara@chiba-u.jp, m38j@icrr.u-tokyo.ac.jp,
sasaki@chiba-u.jp

ABSTRACT: Recently, a violation of the CKM unitarity condition has been reported in the latest charm-meson data and the latest lattice results, once the universal electroweak correction is taken into account. In this article, we analytically derive for the first time the complete one-loop electroweak (EW) and QED corrections to the $D_s^+ \rightarrow \ell^+ \nu_\ell$ decays for $\ell = \mu, \tau$. Our analysis incorporates both short-distance EW-QED corrections, which are beyond the leading-logarithmic approximation (the so-called Sirlin factor), and long-distance soft-photon corrections depending on the maximum total energy of undetected photons with their resummation. Although the inclusive photon QED corrections to the meson leptonic decays are well known, they do not match the actual measurement circumstances in $D_s^+ \rightarrow \mu^+ \nu_\mu$. We find $|V_{cs}|_{D_s} = 0.991 \pm 0.007$ from the latest data on D_s^+ leptonic decays. We show that properly including these radiative corrections is essential to bring the second-column CKM unitarity tests into agreement with the Standard Model expectation. The study emphasizes that the current limiting factor in confirming CKM unitarity is the precision of QED corrections, and it points out that improving lattice simulations, taking the QED corrections into account, would be desirable for a more robust confirmation.

KEYWORDS: CKM Parameters, Charm Physics, Precision QED, Higher Order Electroweak Calculations

Contents

1	Introduction	1
2	Short-distance QED corrections	3
2.1	Corrections to the $cs\ell\nu$ amplitude	4
2.2	Corrections to the Fermi constant	8
2.3	Summary of the short-distance corrections	10
3	Long-distance QED corrections	11
3.1	Soft photon emissions	12
3.2	Virtual corrections	15
3.3	Summary of the long-distance corrections	16
4	Complete radiative corrections to $D_s^+ \rightarrow \ell^+\nu$	18
4.1	Estimation of E_{\max}	18
4.2	PHOTOS QED corrections	21
4.3	Numerical effects to $ V_{cs} $ and CKM unitarity	21
5	Discussion and Conclusions	27
A	Details of the short-distance corrections	28
A.1	Regularization scheme dependence	28
A.2	Matching onto the weak Hamiltonian	28
B	Details of the long-distance corrections	29
B.1	Lagrangian	29
B.2	Dilogarithm formula	29
B.3	Photon energy cut	30
B.4	Inclusive limit	30

1 Introduction

The Cabibbo–Kobayashi–Maskawa (CKM) matrix, V , expresses the mixing among quark flavors and is also known as the only source of (confirmed) CP violation [1]. Within the Standard Model (SM), the unitarity of the CKM matrix

$$VV^\dagger = V^\dagger V = \mathbb{1}, \tag{1.1}$$

is imposed without any question. This unitarity condition arises from the Higgs mechanism, which involves only the Yukawa coupling, generation-independent gauge interactions, the left-handedness of the charged current, and the absence of exotic matter in the full Lagrangian. On the other hand, it is also well known that the SM is not the theory of everything because of, *e.g.*, the matter-antimatter asymmetry in the Universe, and it is expected that New Physics (NP) beyond the SM will emerge at some high energy scale. For instance, in the vector-like quark [2–6] or the vector-like lepton models [7–9], the unitarity of the 3×3 CKM matrix will be violated to some extent.

There are two categories of the unitarity conditions. The first one is the orthogonality conditions:

$$\sum_{k=1}^3 V_{ik} V_{jk}^* = \sum_{k=1}^3 V_{ki} V_{kj}^* = 0 \quad (\text{for } i \neq j), \quad (1.2)$$

which is also called the unitarity triangles. The advantage is that it allows us to verify the consistency of magnitudes of CP-violating observables across different mesons. In particular, the condition of $V_{ud}V_{ub}^* + V_{cd}V_{cb}^* + V_{td}V_{tb}^* = 0$ has been comprehensively studied by the CKMfitter [10, 11] and UTfit collaborations [12, 13], and no indication of NP has been observed, up to now.^{#1} On the other hand, the second category is the normalization conditions:

$$\sum_{k=1}^3 |V_{ik}|^2 = \sum_{k=1}^3 |V_{ki}|^2 = 1. \quad (1.3)$$

Historically, studies of these conditions have been limited compared to the unitarity triangles because the theoretical uncertainties from the form factors have covered the underlying trend, rendering detailed discussion challenging. However, recent progress in lattice QCD simulations significantly reduced these theoretical uncertainties and enabled quantitative analyses of the normalization conditions [19].

In recent years, a notable tension has become clear in the first-row CKM unitarity test: $|V_{ud}|^2 + |V_{us}|^2 + |V_{ub}|^2 - 1 = -(1.51 \pm 0.53) \times 10^{-3}$, where a slight deficit was reported [6]. The corresponding significance is -2.8σ .^{#2} This discrepancy has been referred to as the Cabibbo angle anomaly (CAA) [29, 30]. The test of the CAA has stimulated intense surveys of the QED radiative corrections in the beta decays and kaon decays, including the lattice QCD+QED simulations [31–35]. It should be equally important to extend such unitarity tests to other rows and columns of the CKM matrix.

According to the approach of the Particle Data Group (PDG), the CKM elements $|V_{cd}|$ and $|V_{cs}|$ are extracted from the D and D_s^+ meson leptonic and semi-leptonic decays, using the theoretical knowledge of the form factors. The PDG approach is based on the tree-level

^{#1}Furthermore, the kaon unitarity triangle has also been studied in Refs. [14–18].

^{#2}This significance increases (about $+1\sigma$) when the neutron lifetime data based on the neutron-beam experiments [20] are adopted in the global fit analysis [21]. On the other hand, this tension slightly decreases (about -0.5σ) when a new lattice calculation for the QED correction to the beta decays [22] is used. More recent progress on the QED corrections and the finite nuclear size corrections to the beta decays are provided in Refs. [23–25] and Refs. [26–28], respectively.

matching of the theoretical predictions with the charm-meson measurements because the radiative corrections have not been fully studied. However, it was recently pointed out that once the universal electroweak correction, corresponding to a short-distance correction, is taken into account in the extraction of $|V_{cs}|$, the normalization conditions in Eq. (1.3) are significantly violated at -4.3σ level for the second-row unitarity condition and at -5.2σ level for the second-column one [36].

It is important to note that the Wolfenstein parametrization for the CKM matrix [37] follows strict unitarity to order of λ^3 , while the magnitude of the soft photon correction, corresponding to a long-distance correction, is typically

$$\mathcal{O}(\alpha) \approx \mathcal{O}(\lambda^3) . \quad (1.4)$$

It can occasionally provide nontrivial and sizable corrections exceeding $\mathcal{O}(1)\%$, *e.g.*, the long-distance QED corrections to the lepton flavor universality test [38]. Therefore, such $\mathcal{O}(\alpha)$ corrections can easily ruin the unitarity condition within the Wolfenstein parametrization. In other words, complete one-loop QED corrections are needed in the extractions of the CKM components to check the unitarity condition.

In actual experiments, we will explain later that there is a cut that excludes a hard photon emission in order to collect signals in $D_s^+ \rightarrow \mu^+ \nu_\mu$ process. On the other hand, such a cut does not work in $D_s^+ \rightarrow \tau^+ \nu_\tau$ process. This difference would provide a nontrivial effect for the extraction of $|V_{cs}|$.

In this article, we will analytically study the complete one-loop radiative corrections to $D_s^+ \rightarrow \ell^+ \nu_\ell$ decays. In Sec. 2, we will derive the one-loop analytic formula of the short-distance EW-QED corrections, reproducing the known leading-logarithmic correction, and also obtain a non-logarithmic correction. Furthermore, we discuss the regularization-scheme dependence. In Sec. 3, we will compute the long-distance QED corrections and provide the analytic formulae. In Sec. 4, we will extract the value of $|V_{cs}|$ from the latest data, and investigate the CKM unitarity test. Section 5 is devoted to the conclusions and discussion. Various useful results and further detailed calculations are given in the appendices.

2 Short-distance QED corrections

In this section, we calculate the short-distance EW-QED corrections to the $cs\ell\nu$ amplitude. In order to consistently treat the Fermi coupling constant G_F , the short-distance EW-QED corrections to the muon lifetime are also discussed. Throughout this paper, we use the QED charge defined below:

$$Q_c = \frac{2}{3}, \quad Q_s = -\frac{1}{3}, \quad Q_\ell = -1, \quad Q_\nu = 0. \quad (2.1)$$

Note that thanks to the QCD Ward identity, QCD one-loop corrections are completely canceled among the self-energies and the vertex correction in the $cs\ell\nu$ amplitude, and there is no operator mixing with the other operators in the weak Hamiltonian [39]. The leading QCD correction appears from two-loop level as a mixed QCD-QED correction [40–43]. We will see the impact at the end of this section.

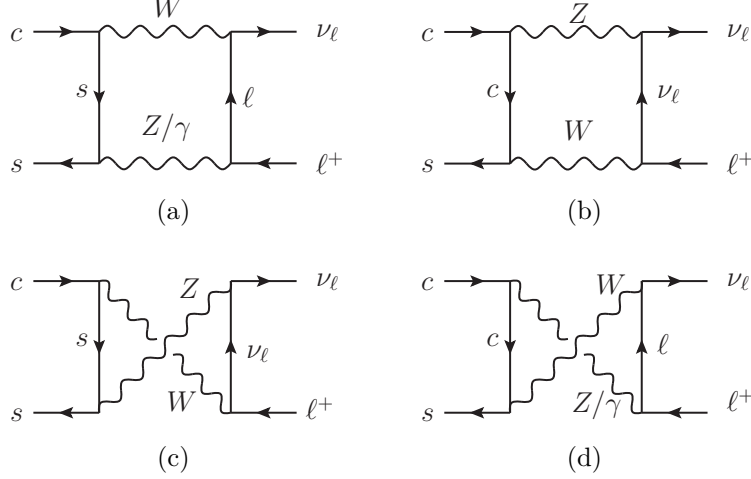


Figure 1: Feynman diagrams for the box contributions.

2.1 Corrections to the $cs\ell\nu$ amplitude

Electroweak corrections. First, we calculate the ZW -box contributions to the $cs\ell\nu$ amplitude. There are four one-loop diagrams shown in Fig. 1, all of which give finite contributions, which therefore are regularization scheme independent. The results for individual diagrams are

$$i\mathcal{M}_{(a)}^{ZW} = i\mathcal{M}_0 \frac{g_Z^2}{16\pi^2} \left(-\frac{1}{2} - Q_s s_W^2 \right) \left(-\frac{1}{2} - Q_\ell s_W^2 \right) \frac{M_W^2}{M_Z^2 - M_W^2} \ln \frac{M_Z^2}{M_W^2} + \mathcal{O} \left(\frac{s}{M_W^2} \right), \quad (2.2)$$

$$i\mathcal{M}_{(b)}^{ZW} = i\mathcal{M}_0 \frac{g_Z^2}{32\pi^2} \left(\frac{1}{2} - Q_c s_W^2 \right) \frac{M_W^2}{M_Z^2 - M_W^2} \ln \frac{M_Z^2}{M_W^2} + \mathcal{O} \left(\frac{s}{M_W^2} \right), \quad (2.3)$$

$$i\mathcal{M}_{(c)}^{ZW} = -i\mathcal{M}_0 \frac{g_Z^2}{8\pi^2} \left(-\frac{1}{2} - Q_s s_W^2 \right) \frac{M_W^2}{M_Z^2 - M_W^2} \ln \frac{M_Z^2}{M_W^2} + \mathcal{O} \left(\frac{s}{M_W^2} \right), \quad (2.4)$$

$$i\mathcal{M}_{(d)}^{ZW} = -i\mathcal{M}_0 \frac{g_Z^2}{4\pi^2} \left(\frac{1}{2} - Q_c s_W^2 \right) \left(-\frac{1}{2} - Q_\ell s_W^2 \right) \frac{M_W^2}{M_Z^2 - M_W^2} \ln \frac{M_Z^2}{M_W^2} + \mathcal{O} \left(\frac{s}{M_W^2} \right), \quad (2.5)$$

where the tree-level amplitude is defined by

$$\mathcal{M}_0 = -\frac{4G_F}{\sqrt{2}} V_{cs}^* (\bar{s} \gamma^\mu P_L c) (\bar{\nu}_\ell \gamma_\mu P_L \ell), \quad (2.6)$$

with $G_F/\sqrt{2} \equiv g^2/8M_W^2$, $g_Z \equiv \sqrt{g^2 + g'^2}$, and the weak-mixing angle in the $\overline{\text{MS}}$ scheme $s_W^2 \equiv \sin^2 \hat{\theta}_W(M_Z) = 0.23129(4)$ [44]. In these calculations, we kept $s = (p_c + p_s)^2$ terms in the loop integrals, and it was found that all of them are suppressed by s/M_W^2 ; When meson decays are considered with $\sqrt{s} = \mathcal{O}(1)$ GeV, these terms are safely negligible in the radiative corrections. Here and throughout, we used the Feynman-'t Hooft gauge for the gauge fixing of the weak gauge boson propagators. Since all the radiative corrections in this study are flavor conserving, the Nambu–Goldstone (NG) boson contributions in the

loop diagrams are always proportional to small Yukawa couplings. So, these contributions are additionally suppressed by m_{light}^2/M_W^2 and are also safely negligible.

The total contribution from the above ZW -box diagrams is

$$\begin{aligned} i\mathcal{M}^{ZW} &\simeq i\mathcal{M}_0 \frac{g_Z^2}{32\pi^2} \left[5 + 5(-Q_c + Q_s + Q_\ell) s_W^2 + 2Q_\ell(-4Q_c + Q_s) s_W^4 \right] \frac{M_W^2}{M_Z^2 - M_W^2} \ln \frac{M_Z^2}{M_W^2} \\ &= i\mathcal{M}_0 \frac{\alpha(M_Z)}{4\pi} \left[Q_\ell(-4Q_c + Q_s) + \frac{5}{2s_W^2} \left(\frac{1}{s_W^2} - Q_c + Q_s + Q_\ell \right) \right] \ln \frac{M_Z^2}{M_W^2}. \end{aligned} \quad (2.7)$$

Here, $4\pi\alpha(M_Z) = g^2 s_W^2$ is the (squared) electromagnetic coupling in the $\overline{\text{MS}}$ scheme and $\alpha(M_Z)^{-1} = 127.930(8)$ [44, 45].

One should note that in traditional calculations, the Fermi coupling constant is related to the renormalized $SU(2)_L$ gauge coupling and W -boson mass as

$$\frac{G_F}{\sqrt{2}} = \frac{g^2}{8M_W^2} (1 + \Delta r), \quad (2.8)$$

where Δr stands for the short-distance radiative corrections to the muon lifetime [46–48], which were evaluated using the naive dimensional regularization (NDR) [49]. For the clarity of the calculations, we do not use this formula; we will instead explicitly compute the short-distance corrections to the muon lifetime in this section and subtract them from our results, whose prescription is equivalent to $(G_F/\sqrt{2})(1 - \Delta r) = g^2/8M_W^2$. This also allows us to discuss the dependence on the regularization schemes.

γW -box contributions. Next, we consider the γW -box contributions. The one-loop diagrams in the full theory are shown in Fig. 1(a) and (d). To regulate the IR singularities coming from the massless photon propagator, here and throughout, we will introduce a tiny nonzero photon mass m_γ . By explicit loop calculations in the full theory, we obtain:

$$\begin{aligned} i\mathcal{M}_{(a)}^{\gamma W} &= -i\mathcal{M}_0 \frac{\alpha}{4\pi} Q_s Q_\ell \left\{ \frac{7}{2} - \ln \left[\frac{2M_W^2}{s(1 - \cos \theta)} \right] + \frac{2\pi^2}{3} + \ln^2 \left[\frac{2m_\gamma^2}{s(1 - \cos \theta)} \right] \right. \\ &\quad \left. + 4 \ln \left[\frac{2m_\gamma^2}{s(1 - \cos \theta)} \right] \right\} + \mathcal{O} \left(\frac{s}{M_W^2} \right), \end{aligned} \quad (2.9)$$

$$\begin{aligned} i\mathcal{M}_{(d)}^{\gamma W} &= i\mathcal{M}_0 \frac{\alpha}{\pi} Q_c Q_\ell \left\{ -\ln \left[\frac{2M_W^2}{s(1 + \cos \theta)} \right] + \frac{\pi^2}{6} + \frac{1}{4} \ln^2 \left[\frac{2m_\gamma^2}{s(1 + \cos \theta)} \right] \right. \\ &\quad \left. + \ln \left[\frac{2m_\gamma^2}{s(1 + \cos \theta)} \right] \right\} + \mathcal{O} \left(\frac{s}{M_W^2} \right), \end{aligned} \quad (2.10)$$

where θ is the angle between the momenta of c and ν_ℓ .

For the one-loop matching onto the weak Hamiltonian at the renormalization scale $\mu \ll M_W$, we need the calculations of the one-loop corrections to the four-fermion operator $(\bar{s}\gamma^\mu P_L c)(\bar{\nu}_\ell \gamma_\mu P_L \ell)$ shown in Fig. 2. These diagrams contain both UV and IR divergences. To assess the UV divergence, we considered two different schemes of the dimensional regularization ($d = 4 - 2\epsilon$), although depending on the regularization schemes the finite terms

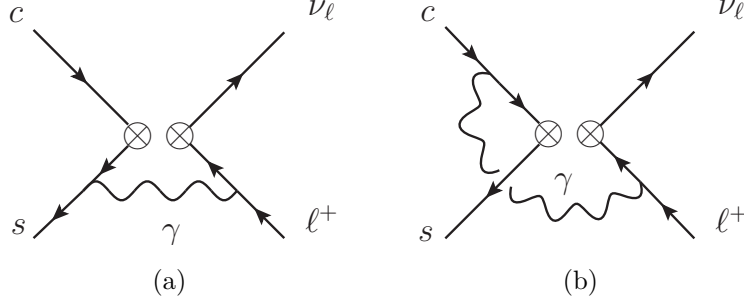


Figure 2: Feynman diagrams for the one-loop matchings onto the $cs\ell\nu$ operator. The vertex “ $\otimes \otimes$ ” denotes the insertion of the four-fermion operator $(\bar{s}\gamma^\mu P_L c)(\bar{\nu}_\ell \gamma_\mu P_L \ell)$.

in the matching conditions are changed. For the one-loop corrections to the operator, we obtain

$$i\mathcal{M}_{(a)}^\gamma = -i\mathcal{M}_0 \frac{\alpha}{4\pi} Q_s Q_\ell \left\{ -\frac{1}{\bar{\epsilon}} + 4 + \kappa_a - \ln \left[\frac{2\mu^2}{s(1 - \cos \theta)} \right] + \frac{2\pi^2}{3} + \ln^2 \left[\frac{2m_\gamma^2}{s(1 - \cos \theta)} \right] + 4 \ln \left[\frac{2m_\gamma^2}{s(1 - \cos \theta)} \right] \right\}, \quad (2.11)$$

$$i\mathcal{M}_{(b)}^\gamma = i\mathcal{M}_0 \frac{\alpha}{\pi} Q_c Q_\ell \left\{ -\frac{1}{\bar{\epsilon}} - \frac{5}{4} + \kappa_b - \ln \left[\frac{2\mu^2}{s(1 + \cos \theta)} \right] + \frac{\pi^2}{6} + \frac{1}{4} \ln^2 \left[\frac{2m_\gamma^2}{s(1 + \cos \theta)} \right] + \ln \left[\frac{2m_\gamma^2}{s(1 + \cos \theta)} \right] \right\}, \quad (2.12)$$

where $1/\bar{\epsilon} \equiv 1/\epsilon - \gamma_E + \ln 4\pi$ and γ_E is the Euler’s constant. The UV divergences ($1/\bar{\epsilon}$) are absorbed by the operator renormalization. The parameters κ_i represent the regularization-scheme-dependent parameters that arise from the treatment of γ_5 in d dimensions. We parameterized them as $\kappa_i = 0$ in the NDR scheme with anticommuting γ_5 . On the other hand, the additional constants $\kappa_a = -2, \kappa_b = 0$ appear in the ’t Hooft–Veltman (HV) scheme with non-anticommuting γ_5 [50–52]. See Appendix A.1 for the scheme dependence.

Compared with these formulae, one can obtain proper one-loop level radiative corrections at the renormalization scale μ , as follows:

$$i\mathcal{M}_{(a)}^{\gamma W} - i\mathcal{M}_{(a)}^\gamma \Big|_{\bar{\epsilon}^0} = i\mathcal{M}_0 \frac{\alpha}{4\pi} Q_s Q_\ell \left[\ln \left(\frac{M_W^2}{\mu^2} \right) + \frac{1}{2} + \kappa_a \right], \quad (2.13)$$

$$i\mathcal{M}_{(d)}^{\gamma W} - i\mathcal{M}_{(b)}^\gamma \Big|_{\bar{\epsilon}^0} = -i\mathcal{M}_0 \frac{\alpha}{\pi} Q_c Q_\ell \left[\ln \left(\frac{M_W^2}{\mu^2} \right) - \frac{5}{4} + \kappa_b \right]. \quad (2.14)$$

Here, the θ and m_γ divergences are thoroughly canceled out as expected. For the details of the loop calculations, see Appendix A.2. The total contribution from the γW -box diagrams is

$$i\mathcal{M}^{\gamma W} = i\mathcal{M}_0 \frac{\alpha}{4\pi} \left[Q_\ell (-4Q_c + Q_s) \ln \left(\frac{M_W^2}{\mu^2} \right) + Q_\ell \left(5Q_c + \frac{1}{2}Q_s \right) + Q_\ell (Q_s \kappa_a - 4Q_c \kappa_b) \right]. \quad (2.15)$$

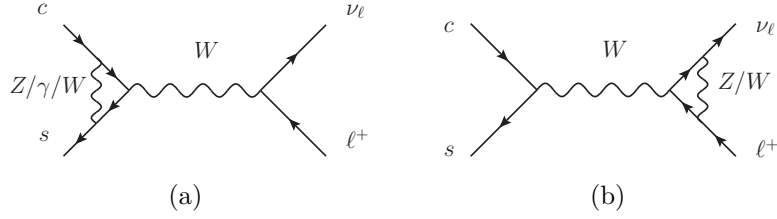


Figure 3: Vertex corrections with virtual gauge bosons attached between fermions.

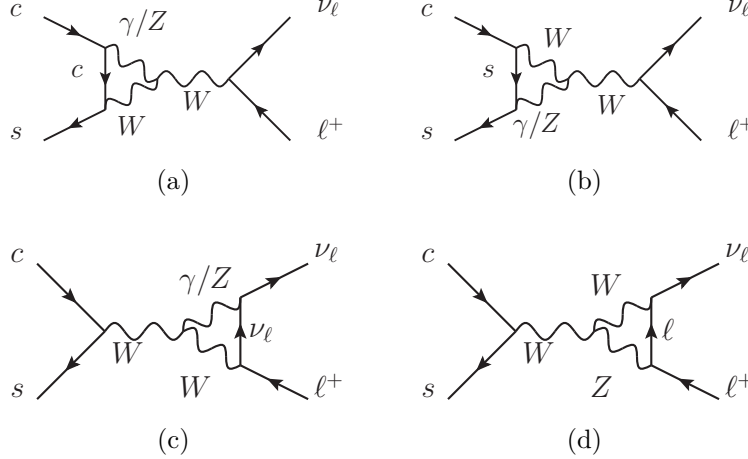


Figure 4: Vertex corrections involving the three-gauge-boson interactions.

Vertex corrections. There are two types of vertex corrections; the vertex corrections shown in Fig. 3 that the virtual gauge bosons couple to fermions, and diagrams shown in Fig. 4 that involve the three-gauge-boson interactions. It is well known that these contributions are completely canceled in total. Let us present this briefly for pedagogical purposes.

First, the photon correction in Fig. 3(a) is completely canceled (with the corresponding one in Fig. 2) in the one-loop matching onto the weak Hamiltonian, *e.g.*, see Ref. [39].

The W corrections in Fig. 3 are equivalent to the ones in the $\mu \rightarrow e \nu_\mu \bar{\nu}_e$ decay. Therefore, as long as G_F is determined by the measurement of the muon lifetime, these corrections can be absorbed by a redefinition of g . The Z corrections are more subtle because the magnitude of the interactions differs between quarks and leptons. However, by adding the contributions from self-energy in Fig. 5(a), these corrections also become absorbable through the redefinition, see the next subsection for details.

Next, for the contributions from Fig. 4, the summation of them cancels each other out, including divergences. In the NDR scheme, the photon corrections in Fig. 4 give

$$\begin{aligned}
 i\mathcal{M}_{\text{vertex}}^\gamma &= i\mathcal{M}_0 \frac{3\alpha}{4\pi} (Q_c - Q_s + Q_\ell) \left[\frac{1}{\epsilon} + \ln \left(\frac{\mu^2}{M_W^2} \right) + \frac{5}{6} + \mathcal{O} \left(\frac{s}{M_W^2} \right) \right] \\
 &\propto Q_c - Q_s + Q_\ell = 0.
 \end{aligned}
 \tag{2.16}$$

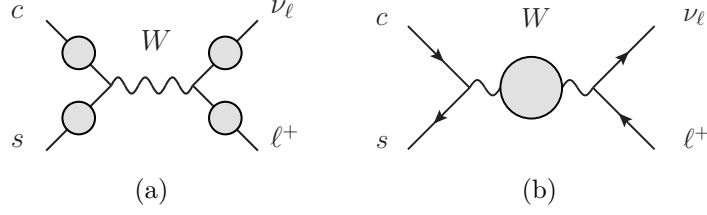


Figure 5: Self-energy diagrams.

Similar cancellation occurs for Z corrections:

$$\begin{aligned} \mathcal{M}_{\text{vertex}}^Z &\propto \left(\frac{1}{2} - Q_c s_W^2 \right) - \left(-\frac{1}{2} - Q_s s_W^2 \right) + \left(-\frac{1}{2} - Q_\ell s_W^2 \right) - \left(\frac{1}{2} \right) \\ &= 0, \end{aligned} \quad (2.17)$$

where each parenthesis corresponds to the left-handed Z couplings.^{#3}

Other contributions. Other contributions in Fig. 5, except for the virtual-photon self-energy diagram of the charged-lepton leg, do not contribute due to the renormalization, see, *e.g.*, Refs. [47, 48]. The self-energy for the charged-lepton leg is classified as the long-distance QED correction and will be calculated in the next section (see Fig. 8).

2.2 Corrections to the Fermi constant

Usually, the Fermi coupling constant $G_F = 1.1663788(6) \times 10^{-5} \text{ GeV}^{-2}$ is derived from the muon lifetime [44]:

$$\tau_\mu^{-1} \equiv \Gamma(\mu \rightarrow e \nu_\mu \bar{\nu}_e(\gamma)) = \frac{G_F^2 m_\mu^5}{192\pi^3} F(\rho) (1 + \Delta q), \quad (2.19)$$

with $\rho = m_e^2/m_\mu^2$, through calculations in the Fermi model where the W propagator is replaced by the Fermi-contact interaction. The function $F(\rho)$ represents the electron mass dependence for the phase space integral: $F(\rho) = 1 - 8\rho + 8\rho^3 - \rho^4 - 12\rho^2 \ln \rho = 0.99981295$. Δq represents the QED corrections and has been evaluated up to $\mathcal{O}(\alpha^3)$ terms [48, 54–61]. The leading terms of the QED corrections were derived by Kinoshita and Sirlin [54],

$$\tau_\mu^{-1} = \frac{G_F^2 m_\mu^5}{192\pi^3} F(\rho) \left[1 + \frac{\alpha(m_\mu)}{2\pi} \left(\frac{25}{4} - \pi^2 \right) \right], \quad (2.20)$$

^{#3}For the HV scheme, we have checked that the cancellation of the vertex corrections in Fig. 4 is not obvious but still correct. In fact, since a contraction of the Dirac matrices: $\gamma_\mu P_R \gamma^\mu \bar{\gamma}^\nu P_L = -2\epsilon \bar{\gamma}^\nu P_L$ holds, where $\bar{\gamma}^\nu$ is the 4-dimensional gamma matrix [53], the right-handed Z interactions provide nonzero contributions multiplying by $1/\epsilon$ pole. We find that this contribution is canceled out by the (right-handed) γ interaction in the HV scheme. For example, we obtained

$$\begin{aligned} i\mathcal{M}_{\text{vertex(b)}}^\gamma + i\mathcal{M}_{\text{vertex(b)}}^Z &\supset i\mathcal{M}_0 \frac{3e}{32\pi^2} \left[eQ_s + g_Z (-Q_s s_W^2) \frac{c_W}{s_W} \right] \\ &= 0, \end{aligned} \quad (2.18)$$

from Fig. 4(b). Here, the factor c_W/s_W comes from WWZ vertex.

which corresponds to the sum of the one-loop virtual photon correction and the inclusive contribution from single-real-photon emission with $m_e = 0$. The important point is that the QED corrections Δq have been calculated using the optical theorem for the muon self-energy diagrams in the Fermi model,^{#4} so that the resultant QED corrections correspond to the inclusive QED radiative correction, with both hard and soft photon emissions contained. This fact implies that all short-distance corrections to the muon lifetime in the full theory have to be conventionally absorbed in the definition of G_F .

Therefore, in order to calculate the full one-loop radiative corrections to the meson decays consistently, one must also know the complete radiative corrections to the muon lifetime in the full theory as well. To be more precise, the short-distance QED and EW corrections to the $\mu\nu_\mu e\nu_e$ operator must be calculated, and we will subtract them from the above results. Fortunately, we can readily obtain them from the calculations in the case of the meson leptonic decays.

First, ZW -box contributions come from the same diagrams as Fig. 1, where the strange and charm quark lines are replaced by the muon and muon-neutrino, respectively. The result can be obtained from Eq. (2.7) by replacing $Q_c \rightarrow Q_\nu$ and $Q_s \rightarrow Q_\ell$, as

$$i\mathcal{M}_{\text{muon}}^{ZW} = i\mathcal{M}_0^{\text{muon}} \frac{\alpha(M_Z)}{4\pi} \left[Q_\ell^2 + \frac{5}{2s_W^2} \left(\frac{1}{s_W^2} + 2Q_\ell \right) \right] \ln \frac{M_Z^2}{M_W^2}, \quad (2.21)$$

with $\mathcal{M}^{\text{muon}} = -4G_F/\sqrt{2}(\bar{\mu}\gamma^\mu P_L\nu_\mu)(\bar{\nu}_e\gamma_\mu P_L e)$. This result is consistent with Refs. [41, 62].

Next, γW -box contribution comes from only Fig. 1(a) type. Since the virtual photon correction in Δq for the Fermi model corresponds to Fig. 2(a) type, which is already included in Eq. (2.19), we have to subtract this contribution. So, the short-distance γW -box contribution to the muon lifetime is

$$\begin{aligned} i\mathcal{M}_{\text{muon}}^{\gamma W} &= i\mathcal{M}_{\text{muon(a)}}^{\gamma W} - i\mathcal{M}_{\text{muon(a)}}^\gamma \Big|_{\epsilon^0} \\ &= i\mathcal{M}_0^{\text{muon}} \frac{\alpha}{4\pi} Q_\ell^2 \left[\ln \left(\frac{M_W^2}{\mu^2} \right) + \frac{1}{2} + \kappa_a \right]. \end{aligned} \quad (2.22)$$

Similar to the previous subsection, the photon vertex corrections do not give a contribution to the muon lifetime.

In practice, the other weak radiative corrections also contribute to the muon lifetime. These radiative corrections are called the universal renormalization factor [41, 62]. An important fact is that they are also contained within the four-fermion interactions for the meson (semi-)leptonic decays in exactly the same form. As the most nontrivial check of this cancellation, we have explicitly calculated the Z -boson radiative corrections to the muon/neutrino wave function renormalization constants (in Fig. 5(a) type) and the muon-neutrino- Z triangle diagram (in Fig. 3(a) type), using the NDR scheme for the UV

^{#4}It was shown that the IR poles and the singularities as $m_e \rightarrow 0$ are canceled in the amplitude level, and the the UV divergences are absorbed by the on-shell renormalization in the optical theorem prescription [56].

divergences. By adding these contributions to the muon decays together, we obtain

$$i\mathcal{M} = -i\mathcal{M}_0^{\text{muon}} \frac{g_z^2}{32\pi^2} \left[1 + (Q_\ell - Q_\nu) s_W^2 \right]^2 \left[\frac{1}{\epsilon} + \ln \left(\frac{\mu^2}{M_Z^2} \right) - \frac{1}{2} \right], \quad (2.23)$$

where we discarded the contributions from the $e\nu_e$ side (that is trivially universal compared to the meson (semi-)leptonic decay amplitudes).

On the other hand, in the D_s^+ leptonic decays, corresponding virtual- Z contributions can be obtained by replacing $Q_\nu \rightarrow Q_c$ and $Q_\ell \rightarrow Q_s$. They lead to the exact same corrections. Therefore, these weak corrections, including the UV divergence, are classified as the universal renormalization factor, and do not contribute to the D_s^+ meson leptonic decay rate [48].

Hence, the universal contributions necessarily cancel in the meson (semi-)leptonic decays in total, as long as the Fermi coupling constant is defined by Eq. (2.19). This feature is expected to be independent of the regularization scheme.

2.3 Summary of the short-distance corrections

Collecting the contributions obtained above, we arrive at the short-distance EW-QED corrections to the $cs\ell\nu$ amplitude:

$$\begin{aligned} \mathcal{M}^{\text{SD}} &= \mathcal{M}_0 + \mathcal{M}^{ZW} + \mathcal{M}^{\gamma W} - \mathcal{M}_{\text{muon}}^{ZW} - \mathcal{M}_{\text{muon}}^{\gamma W} \\ &= \mathcal{M}_0 \left(1 + \frac{\alpha(\mu)}{4\pi} \left\{ Q_\ell (-4Q_c + Q_s - Q_\ell) \ln \left(\frac{M_Z^2}{\mu^2} \right) + Q_\ell \left(5Q_c + \frac{1}{2}Q_s - \frac{1}{2}Q_\ell \right) \right. \right. \\ &\quad \left. \left. + Q_\ell [(Q_s - Q_\ell) \kappa_a - 4Q_c \kappa_b] \right\} \right). \end{aligned} \quad (2.24)$$

Here, the renormalization group of $\alpha(\mu)$ was not explicitly addressed in our discussion. Since its scale dependence is small (in view of the precision of the charm physics), we naively take $\alpha(\mu)$ as the overall factor of the short-distance corrections, and two logarithmic terms are merged into a single term [63].

As mentioned at the beginning of this section, the QCD corrections appear at two-loop level [40–43]. Combining with the QCD correction (\mathcal{A}_{g_s}) and substituting the QED charge in Eq. (2.24), we eventually obtain the short-distance corrections

$$\eta_{\text{EW}} \equiv \frac{\mathcal{M}}{\mathcal{M}_0} = \begin{cases} 1 + \frac{\alpha(\mu)}{2\pi} \left[\ln \left(\frac{M_Z^2}{\mu^2} \right) + \frac{1}{2} \mathcal{A}_{g_s} - \frac{11}{6} \right] & (\text{NDR}), \\ 1 + \frac{\alpha(\mu)}{2\pi} \left[\ln \left(\frac{M_Z^2}{\mu^2} \right) + \frac{1}{2} \mathcal{A}_{g_s} - \frac{7}{6} \right] & (\text{HV}), \end{cases} \quad (2.25)$$

with $\mu = m_{D_s}$ for the D_s^+ leptonic decay.^{#5} In the numerical study in Sec. 4, we use $\alpha(m_{D_s})^{-1} \simeq \alpha(m_\tau)^{-1} = 133.450(6)$ [44]. For the QCD correction, we use a numerical

^{#5}The numerical values are

$$\eta_{\text{EW}} = \begin{cases} 1.0068 & (\text{NDR}), \\ 1.0076 & (\text{HV}), \end{cases} \quad (2.26)$$

for the D_s^+ leptonic decays.

value for $\mathcal{O}(1)$ GeV meson and β decays, evaluated from Refs. [41, 43],^{#6}

$$\mathcal{A}_{g_s} = -0.34. \quad (2.27)$$

The leading-logarithmic term is consistent with the well-known short-distance electroweak correction known as the Sirlin factor [41, 65]. The $-11/6$ term has been derived in Refs. [66, 67] and Ref. [63] independently. Both works regularize the photon-induced IR divergences by using dimensional regularization with the NDR scheme and setting all external momenta to zero. To the best of our knowledge, this is the first explicit determination of these rational terms using different regularization schemes. We observed that including these rational terms reduces the leading-logarithmic correction by 24% and 15% in the NDR and HV schemes, respectively. It is also noted that the difference between the two regularization schemes is small.

In standard treatments of QCD corrections, such scheme dependence at $\mu = M_W$ is canceled by incorporating the two-loop QCD anomalous dimensions of the operators, while the scheme dependence at the low energy matching scale (the hadronic scale) remains, but can be compensated by the change in μ [14]. In our approximate approach, we use a fixed value of α and therefore do not take the QED anomalous dimensions into account. If we consider that the difference between two short-distance corrections in Eq. (2.25) can be traded for a change of μ , then choosing

$$\mu_{\text{HV}} = e^{1/3} \mu_{\text{NDR}} \simeq 1.4 \mu_{\text{NDR}} \quad (2.28)$$

yields identical short-distance corrections in the two schemes.

Furthermore, it is found that the QCD correction \mathcal{A}_{g_s} increases $|V_{cs}|$ by just 2×10^{-4} . Since this is an order of magnitude smaller than the numerical value currently under consideration, it can be safely neglected.

We should note that the obtained short-distance corrections in Eq. (2.25) can be applied to *any* meson leptonic and semi-leptonic decays within the SM.

3 Long-distance QED corrections

In this section, we compute the long-distance QED corrections to the $D_s^+ \rightarrow \ell^+ \nu_\ell$ decays using the point-like approximation, *i.e.*, scalar QED (SQED), for the D_s^+ meson state. Based on the definition of the decay constant,

$$\langle 0 | \bar{s} \gamma^\mu \gamma_5 c | D_s^+(p) \rangle = i f_{D_s} p^\mu, \quad (3.1)$$

we matched the effective Lagrangian as follows:

$$\mathcal{L}_{\text{eff}} = \mathcal{L}_{\text{SQED}} - \frac{G_F}{\sqrt{2}} V_{cs}^* f_{D_s} \bar{\nu}_\ell \gamma^\mu (1 - \gamma_5) \ell D_\mu \phi^+ + \text{h.c.}, \quad (3.2)$$

^{#6}In the pion decays, the QCD correction was estimated as $\mathcal{A}_{g_s} = -(\alpha_s/\pi) \ln(M_Z/m_\rho)$ [64].

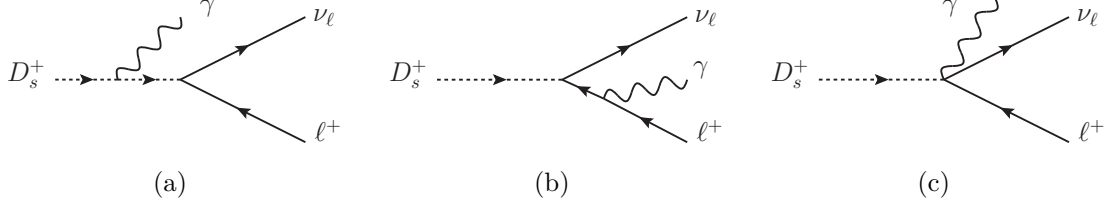


Figure 6: Feynman diagrams for the real photon emissions.

where ϕ^+ is a complex scalar field that indicates D_s^+ . $\mathcal{L}_{\text{SQED}}$ is the corresponding SQED Lagrangian for ϕ^+ , and the covariant derivatives are defined as

$$D_\mu \phi^+ = (\partial_\mu + iQ_{D_s} e A_\mu) \phi^+, \quad (3.3)$$

with $Q_{D_s} = 1$. Note that this matching produces a dimension-five contact interaction $\bar{\nu}_\ell A P_L \ell \phi^+$, which is required to obtain the gauge-invariant radiative corrections [68–70]. A global average of the decay constant for $N_f = 2 + 1 + 1$ is $f_{D_s} = 249.9(0.5)$ MeV [19]. Note that the isospin-breaking correction is currently missing in the lattice calculations.

Performing direct lattice calculations of the QED corrections to the decay constant f_{D_s} remains challenging [71–73]. These works investigated the contribution from a single real-photon emission with $E_\gamma > 10$ MeV, by evaluating hadronic matrix elements with one electromagnetic current insertion. These QED corrections are classified as the *structure-dependent* part of the real radiations. It was found that this structure-dependent part is sizable only in the electron mode $D_s^+ \rightarrow e^+ \nu_\ell \gamma$, whereas for μ and τ modes, the QED corrections are dominated by the point-like contribution, which should correspond to our estimation in the next subsection. Regarding the structure-dependent part of the virtual corrections, we will comment on them in Sec. 5.

3.1 Soft photon emissions

First, we calculate corrections from real soft-photon emissions. As briefly stated in the Introduction, for the μ mode, there is a cut that excludes hard photons from the signal [74–76]. Therefore, we have to analyze the *exclusive* $D_s^+ \rightarrow \mu^+ \nu_\mu \gamma$ decay, which depends on the undetected photon energy. (We will perform resummation for the missing photons.) On the other hand, for the τ mode, the circumstances are different. Both because the mass difference is small between D_s^+ and τ lepton,

$$m_{D_s} - m_\tau \simeq 191 \text{ MeV}, \quad (3.4)$$

and because the decay of τ^+ always produces at least one additional neutrino ($\bar{\nu}_\tau$), the measurements are, in practice, *inclusive* with respect to the soft-photon emissions [76–80]. We will discuss these in detail in Sec. 4.1. It is well-known that for the inclusive observables, the total QED correction has to be suppressed by the cancellations and its magnitude is expected to be $\mathcal{O}(\alpha/\pi)$, *e.g.*, Eq. (2.20) (Kinoshita-Lee-Nauenberg theorem [81, 82]). In contrast, the QED correction can be enhanced in the exclusive decays by the large logarithmic terms that arise from significant differences among the small undetected

photon energy, the light lepton mass, and the meson masses. So, we should expect that the total QED correction is significant in the μ mode, but not in the τ mode.

Diagrams of the (single) photon emissions (with the momentum k), which are also known as the inner-bremsstrahlung, are shown in Fig. 6, and these matrix elements can be simplified as follows:

$$i\mathcal{M}_{\text{real}}^{(a)} = -i\mathcal{M}_0 e Q_{D_s} \frac{p_{D_s} \cdot \epsilon^*(k)}{p_{D_s} \cdot k - i\epsilon}, \quad (3.5)$$

$$i\mathcal{M}_{\text{real}}^{(b)} = -i\mathcal{M}_0 e Q_\ell \frac{p_\ell \cdot \epsilon^*(k)}{p_\ell \cdot k + i\epsilon} - e Q_\ell \frac{G_F}{\sqrt{2}} V_{cs}^* f_{D_s} \bar{u}_{\nu_\ell} (1 + \gamma_5) \left(\frac{m_\ell \not{k}}{2p_\ell \cdot k + i\epsilon} - 1 \right) \not{\epsilon}^*(k) v_\ell, \quad (3.6)$$

$$i\mathcal{M}_{\text{real}}^{(c)} = e Q_{D_s} \frac{G_F}{\sqrt{2}} V_{cs}^* f_{D_s} \bar{u}_{\nu_\ell} (1 + \gamma_5) \not{\epsilon}^*(k) v_\ell, \quad (3.7)$$

where the tree-level amplitude \mathcal{M}_0 is defined by

$$\mathcal{M}_0 = -i \frac{G_F}{\sqrt{2}} V_{cs}^* f_{D_s} m_\ell \bar{u}_{\nu_\ell} (1 + \gamma_5) v_\ell. \quad (3.8)$$

The sum of these three amplitudes is [83]

$$i\mathcal{M}_{\text{real}} = -i\mathcal{M}_0 e \left(Q_{D_s} \frac{p_{D_s} \cdot \epsilon^*}{p_{D_s} \cdot k - i\epsilon} + Q_\ell \frac{p_\ell \cdot \epsilon^*(k)}{p_\ell \cdot k + i\epsilon} \right) - e Q_\ell \frac{G_F}{\sqrt{2}} V_{cs}^* f_{D_s} \frac{m_\ell}{2p_\ell \cdot k + i\epsilon} \bar{u}_{\nu_\ell} (1 + \gamma_5) \not{k} \not{\epsilon}^* v_\ell. \quad (3.9)$$

Although the matrix element $\mathcal{M}_{\text{real}}^{(c)}$ is canceled by part of $\mathcal{M}_{\text{real}}^{(b)}$ in the real photon emission amplitude, this vertex must be kept for the full virtual correction; see the next subsection. The first line in Eq. (3.9) collects the leading soft-photon contribution containing the infrared (IR) divergence, whereas the second line is a subleading term whose contribution is significant only for hard photons. Because the total amplitude of the inner-bremsstrahlung is still proportional to the lepton mass, it receives the helicity suppression.

Taking the spin and polarization sums for the final state particles, we obtain

$$\begin{aligned} \sum_{s,\lambda} |\mathcal{M}_{\text{real}}|^2 &= 4G_F^2 |V_{cs}|^2 f_{D_s}^2 m_\ell^2 e^2 \\ &\times \left\{ - (p_\ell \cdot p_{\nu_\ell}) \left[Q_{D_s} Q_\ell \frac{2p_{D_s} \cdot p_\ell}{(p_{D_s} \cdot k)(p_\ell \cdot k)} + Q_{D_s}^2 \frac{m_{D_s}^2}{(p_{D_s} \cdot k)^2} + Q_\ell^2 \frac{m_\ell^2}{(p_\ell \cdot k)^2} \right] \right. \\ &\quad + Q_\ell^2 \frac{p_{\nu_\ell} \cdot k}{p_\ell \cdot k} - Q_\ell^2 \frac{m_\ell^2 (p_{\nu_\ell} \cdot k)}{(p_\ell \cdot k)^2} - Q_\ell Q_{D_s} \frac{p_\ell \cdot p_{\nu_\ell}}{p_\ell \cdot k} \\ &\quad \left. + Q_\ell Q_{D_s} \frac{p_{D_s} \cdot p_{\nu_\ell}}{p_{D_s} \cdot k} - Q_\ell Q_{D_s} \frac{(p_{D_s} \cdot p_\ell)(p_{\nu_\ell} \cdot k)}{(p_{D_s} \cdot k)(p_\ell \cdot k)} \right\}, \quad (3.10) \end{aligned}$$

where the $\pm i\epsilon$ terms have been omitted for clarity. The terms in the square bracket contain the IR singularity. For the analytic phase space integral, we use the Dalitz plot formalism,

see Appendix B.3. In the IR limit, which corresponds to the two-body decay phase space integral for $\ell^+\nu_\ell$, it is hard to perform the Dalitz integration, so we use the soft-photon approximation [84–86], namely:

$$\int_{E_\gamma < E_{\max}} \frac{d^3\mathbf{k}}{(2\pi)^3} \frac{1}{2E_\gamma} \int d\Pi_2 = \frac{1}{8\pi^2} \int_{m_\gamma}^{E_{\max}} dE_\gamma \sqrt{E_\gamma^2 - m_\gamma^2} \int_{-1}^1 d\cos\theta \int d\Pi_2, \quad (3.11)$$

where m_γ is the soft photon mass introduced to regulate the IR divergences. $\int d\Pi_2$ is the usual two-body phase space. Here, E_{\max} represents the maximum energy of the undetected soft photon in the D_s^+ rest frame. After performing the three-body analytic integrations [44], we obtain the following QED corrections from the single photon radiation:

$$\begin{aligned} \left. \frac{\Gamma(D_s^+ \rightarrow \ell^+ \nu_\ell \gamma)}{\Gamma_0} \right|_{E_\gamma < E_{\max}} &= \frac{\alpha_0}{2\pi} \left\{ -4 \left[1 + \frac{1+x_\ell}{2(1-x_\ell)} \ln x_\ell \right] \ln \left(\frac{2E_{\max}}{m_\gamma} \right) \right. \\ &\quad \left. + 2 - \frac{1+x_\ell}{1-x_\ell} \left[\ln x_\ell + \frac{1}{2} \ln^2 x_\ell + 2\text{Li}_2(1-x_\ell) \right] \right. \\ &\quad \left. + F^{\text{hard}}(E_{\max}) \right\}, \end{aligned} \quad (3.12)$$

with the tree-level partial decay width

$$\Gamma_0 = \frac{G_F^2}{8\pi} |V_{cs}|^2 m_{D_s} m_\ell^2 f_{D_s}^2 (1-x_\ell)^2, \quad (3.13)$$

and the hard-photon correction

$$\begin{aligned} F^{\text{hard}}(E_{\max}) &= \frac{\alpha_0}{2\pi} \left\{ \frac{E_{\max}}{m_{D_s}(1-x_\ell)^2} \left[11 - 14x_\ell - \frac{3E_{\max}}{m_{D_s}} + 4(1-x_\ell) \ln x_\ell - \frac{2E_{\max}}{m_{D_s}} \ln x_\ell \right] \right. \\ &\quad \left. + \frac{1}{(1-x_\ell)^2} \left[\frac{3}{2} - 3x_\ell - 4(1-x_\ell) \frac{E_{\max}}{m_{D_s}} + \frac{2E_{\max}^2}{m_{D_s}^2} \right] \ln \left(1 - \frac{2E_{\max}}{m_{D_s}} \right) \right. \\ &\quad \left. - 2 \left(\frac{1+x_\ell}{1-x_\ell} \right) \text{Li}_2 \left(\frac{2E_{\max}}{m_{D_s}} \right) \right\}, \end{aligned} \quad (3.14)$$

where $x_\ell = m_\ell^2/m_{D_s}^2$. Here, for the long-distance QED corrections, we use the fine-structure constant $\alpha_0^{-1} = 137.035999178(8)$ [44]. The first line of Eq. (3.12) gives $\mathcal{O}(\ln E_{\max})$ contributions (including the IR singularity), and the second line provides a constant correction as $\mathcal{O}((E_{\max})^0)$. The terms in the square bracket in Eq. (3.10) with the soft-photon approximation in Eq. (3.11) precisely provide these two contributions. On the other hand, the third line of Eq. (3.12), F^{hard} , corresponds to $\mathcal{O}(E_{\max})$ contribution, which is usually discarded in the soft-photon approximation. Note that F^{hard} vanishes in the soft photon limit, $F^{\text{hard}}(E_{\max} \rightarrow 0) = 0$. We will show later that the contributions from F^{hard} are tiny. (In Sec. 4.1, we will provide a detailed discussion of the dependence of E_{\max} and how E_{\max} is handled in the experimental analyses.) The analytic formula of F^{hard} is consistent with Eq. (50) of Ref. [31].^{#7}

^{#7}We appreciate Toru Goto for an independent check of the formulae in this subsection.

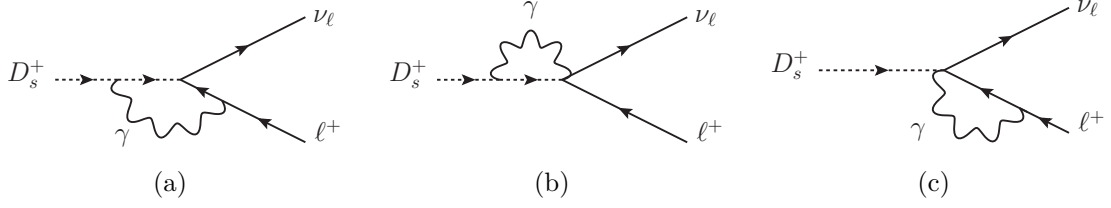


Figure 7: Virtual vertex corrections for the long-distance QED correction.

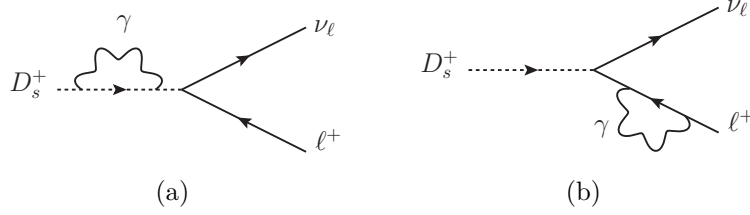


Figure 8: Self-energy diagrams.

As a nontrivial check, we have confirmed the inclusive limit of photon emission, $E_{\max} = (m_{D_s}^2 - m_\ell^2)/2m_{D_s}$. We found that our result is consistent with a famous result by Kinoshita for the fully inclusive inner-bremsstrahlung process of $\pi^+ \rightarrow e^+ \nu_e \gamma$ [87] (for details, see Appendix B.4).

3.2 Virtual corrections

Next, we calculate the virtual corrections to $D_s^+ \rightarrow \ell^+ \nu_\ell$, which are comprised of the vertex corrections in Fig. 7 and the self-energy diagrams in Fig. 8. Both contributions contain the IR singularities, and they must be canceled out when added to the contributions from the soft-photon emissions, as explicitly shown in the next subsection. Regulating the singularities by the soft-photon mass, we obtained each result for the vertex corrections,

$$\begin{aligned} \frac{\Delta\Gamma_{(\text{vertex})}^{(a)}}{\Gamma_0} = & -Q_\ell Q_{D_s} \frac{\alpha_0}{2\pi} \left[\frac{5}{2} \left(\frac{1}{\bar{\epsilon}} + \ln \frac{\mu^2}{m_{D_s}^2} \right) + \frac{11}{2} + \kappa_c \right. \\ & \left. - 2 \left(\frac{1+x_\ell}{1-x_\ell} \right) \ln x_\ell \ln \frac{m_\gamma}{\sqrt{m_{D_s} m_\ell}} - \frac{2}{1-x_\ell} \ln x_\ell \right], \end{aligned} \quad (3.15)$$

$$\frac{\Delta\Gamma_{(\text{vertex})}^{(b)}}{\Gamma_0} = Q_{D_s}^2 \frac{\alpha_0}{2\pi} \left[-\frac{3}{2} \left(\frac{1}{\bar{\epsilon}} + \ln \frac{\mu^2}{m_{D_s}^2} \right) - \frac{7}{2} \right], \quad (3.16)$$

$$\frac{\Delta\Gamma_{(\text{vertex})}^{(c)}}{\Gamma_0} = -Q_\ell Q_{D_s} \frac{\alpha_0}{2\pi} \left[-3 \left(\frac{1}{\bar{\epsilon}} + \ln \frac{\mu^2}{m_\ell^2} \right) - 4 + \kappa_d \right], \quad (3.17)$$

and for the wave-function renormalization constants,

$$\begin{aligned}\frac{\Delta\Gamma_{(\text{self})}^{(a)}}{\Gamma_0} &= 2 \left(\frac{1}{2} \frac{d\Sigma}{dp^2} \Big|_{p^2=m_{D_s}^2} \right) \\ &= Q_{D_s}^2 \frac{\alpha_0}{2\pi} \left(\frac{1}{\bar{\epsilon}} + \ln \frac{\mu^2}{m_{D_s}^2} - 2 \ln \frac{m_\gamma}{\sqrt{m_{D_s} m_\ell}} - \frac{1}{2} \ln x_\ell \right),\end{aligned}\quad (3.18)$$

$$\begin{aligned}\frac{\Delta\Gamma_{(\text{self})}^{(b)}}{\Gamma_0} &= 2 \left(\frac{1}{2} \frac{d\Sigma}{d\cancel{p}} \Big|_{\cancel{p}=m_\ell} \right) \\ &= Q_\ell^2 \frac{\alpha_0}{2\pi} \left[-\frac{1}{2} \left(\frac{1}{\bar{\epsilon}} + \ln \frac{\mu^2}{m_\ell^2} \right) - 2 - 2 \ln \frac{m_\gamma}{\sqrt{m_{D_s} m_\ell}} + \frac{1}{2} \ln x_\ell \right],\end{aligned}\quad (3.19)$$

where Σ denotes the self-energy amplitudes for the external legs. To regulate UV divergence, we use dimensional regularization, with κ_c and κ_d as regularization-scheme-dependent parameters. Again, in the same manner as short-distance calculations, we parametrized $\kappa_c = \kappa_d = 0$ in the NDR scheme,^{#8} while $\kappa_c = 1$ and $\kappa_d = -1$ in the HV scheme. Note that $\Gamma_{(\text{vertex})}^{(b)}$ and the wave-function renormalization constants are common to both schemes. Here, we use the on-shell renormalization, and the renormalized masses are set equal to their physical masses.

The renormalization scale μ should be chosen at the matching scale to the UV theory, namely, the characteristic scale of the structure-dependent radiative corrections in the present study. Because such effects are not incorporated in this paper, the remaining μ -dependence is treated as theoretical uncertainty for the extraction of $|V_{cs}|$, and we drop the $1/\bar{\epsilon}$ terms.

Unexpectedly, we find that the contributions from κ_c and κ_d are canceled in the HV scheme. Hence, total virtual corrections are scheme-independent between the NDR and HV schemes.

3.3 Summary of the long-distance corrections

Combining the contributions from the single photon radiations and the virtual corrections, we derive the long-distance QED corrections to $\Gamma(D_s^+ \rightarrow \ell^+ \nu_\ell)$, and classify them into the corrections from the initial state radiation (ISR), final state radiation (FSR), interference contributions between the ISR and FSR (INT), hard-photon contributions (hard), and other virtual corrections, as follows:

$$\begin{aligned}\frac{\Gamma(D_s^+ \rightarrow \ell^+ \nu_\ell)^{\text{LD}}}{\Gamma_0} &= 1 + \frac{\Delta\Gamma_{(\text{vertex})}^{(a+b+c)}}{\Gamma_0} + \frac{\Delta\Gamma_{(\text{self})}^{(a+b)}}{\Gamma_0} + \frac{\Gamma(D_s^+ \rightarrow \ell^+ \nu_\ell \gamma)}{\Gamma_0} \Big|_{E_\gamma < E_{\text{max}}} \\ &= 1 + F^{\text{ISR}} + F^{\text{FSR}} + F^{\text{INT}} + F^{\text{hard}} + H^{(a)} + H^{(b+c)},\end{aligned}\quad (3.20)$$

where corrections F represent the real photon emissions, while H represent the virtual corrections. (The corrections from the wave-function renormalization constants are included

^{#8}The result of the virtual corrections is consistent with, *e.g.*, Ref. [88]

in $H^{(a)}$.) Each contribution is infrared-safe and is defined in a finite manner^{#9} as follows:

$$F^{\text{ISR}} = \frac{\alpha_0}{2\pi} \left(-2 \ln \frac{2E_{\text{max}}}{\sqrt{m_{D_s} m_\ell}} + 2 \right), \quad (3.21)$$

$$F^{\text{FSR}} = \frac{\alpha_0}{2\pi} \left(-2 \ln \frac{2E_{\text{max}}}{\sqrt{m_{D_s} m_\ell}} - \frac{1+x_\ell}{1-x_\ell} \ln x_\ell \right), \quad (3.22)$$

$$F^{\text{INT}} = \frac{\alpha_0}{2\pi} \left\{ -2 \left(\frac{1+x_\ell}{1-x_\ell} \right) \ln x_\ell \ln \frac{2E_{\text{max}}}{\sqrt{m_{D_s} m_\ell}} - \frac{1+x_\ell}{1-x_\ell} \left[\frac{1}{2} \ln^2 x_\ell + 2\text{Li}_2(1-x_\ell) \right] \right\}, \quad (3.23)$$

$$H^{(a)} = \frac{\alpha_0}{2\pi} \left(3 \ln \frac{\mu^2}{m_{D_s} m_\ell} - \frac{2x_\ell}{1-x_\ell} \ln x_\ell + \frac{7}{2} \right), \quad (3.24)$$

$$H^{(b+c)} = \frac{\alpha_0}{2\pi} \left(-\frac{9}{2} \ln \frac{\mu^2}{m_{D_s} m_\ell} + \frac{3}{4} \ln x_\ell - \frac{15}{2} \right), \quad (3.25)$$

and F^{hard} is defined in Eq. (3.14). Note that these results are the same in both the NDR and HV schemes, as discussed in the previous subsection.

Furthermore, we carry out a resummation of the potentially large contributions of $\mathcal{O}(\alpha^n \ln^n E_{\text{max}})$, which come from the emission of n soft photons. This resummation is also required to remove the $E_{\text{max}} \rightarrow 0$ singularity. The resummation of the soft-photon emissions is accomplished through the replacement of the following terms with an exponential factor Ω_B [38, 85, 86],

$$\begin{aligned} 1 + F^{\text{ISR}} + F^{\text{FSR}} + F^{\text{INT}} &\ni 1 + \frac{\alpha_0}{2\pi} \left[-4 - 2 \left(\frac{1+x_\ell}{1-x_\ell} \right) \ln x_\ell \right] \ln \left(\frac{2E_{\text{max}}}{\sqrt{m_{D_s} m_\ell}} \right) \\ &\xrightarrow{\text{resum.}} \left(\frac{2E_{\text{max}}}{\sqrt{m_{D_s} m_\ell}} \right)^{-\frac{2\alpha_0}{\pi} \left(1 + \frac{1}{2} \frac{1+x_\ell}{1-x_\ell} \ln x_\ell \right)} \\ &\equiv \Omega_B(E_{\text{max}}). \end{aligned} \quad (3.26)$$

Here, E_{max} should be reinterpreted as the maximum total energy of undetected soft photons. We consider this resummation effect when $|V_{cs}|$ is extracted from the data. We will present a numerical comparison of the individual contributions of the long-distance QED corrections in the next section.

^{#9}Both the real photon emissions and the virtual corrections initially have the IR singularities. By transposing the terms proportional to $\ln(m_\gamma/\sqrt{m_{D_s} m_\ell})$ from the virtual corrections to the real photon emissions, we cancel the singularities and express finite results.

4 Complete radiative corrections to $D_s^+ \rightarrow \ell^+ \nu$

Finally, we obtain the complete one-loop QED corrections to $D_s^+ \rightarrow \ell^+ \nu_\ell$ by combining the short- and long-distance corrections in the NDR scheme,

$$\begin{aligned} \Gamma(D_s^+ \rightarrow \ell^+ \nu_\ell) = & \Gamma_0 \left\{ 1 + \frac{\alpha(m_{D_s})}{2\pi} \left[\ln \left(\frac{M_Z^2}{m_{D_s}^2} \right) + \frac{1}{2} \mathcal{A}_{g_s} - \frac{11}{6} \right] \right\}^2 \\ & \times \Omega_B \left\{ 1 + \frac{\alpha_0}{2\pi} \left[-2 - \frac{1+x_\ell}{1-x_\ell} \left(\frac{1}{2} \ln^2 x_\ell + 2 \text{Li}_2(1-x_\ell) \right) \right. \right. \\ & \left. \left. - \frac{3}{2} \ln \frac{\mu^2}{m_{D_s} m_\ell} - \frac{1+15x_\ell}{4(1-x_\ell)} \ln x_\ell \right] + F^{\text{hard}} \right\}. \end{aligned} \quad (4.1)$$

In the HV scheme, the term of $-11/6$ in the first line is replaced by $-7/6$ (see Eq. (2.25)). Note that the structure-dependent QED radiative corrections are currently missing from this formula, which will be discussed in Sec. 5. In this section, we extract the state-of-the-art value of $|V_{cs}|$ from the latest data, and consider the CKM unitarity test.

4.1 Estimation of E_{max}

Before examining the numerical details, we first discuss the experimental circumstances for the value of E_{max} , which is a crucial parameter in the numerical calculation of the long-distance QED corrections. In the experiments, the threshold energy of the electromagnetic calorimeter to detect the photons is $\mathcal{O}(10)$ MeV, in order to tag the $\pi^0 \rightarrow 2\gamma$ events. But, this value does not correspond to E_{max} . In practice, since the beamline radiates a large number of photons, one has to isolate the signal by applying dedicated cuts that effectively ignore many visible soft photons. Although different experiments adopt different selection cuts, here we consider one of the cuts used by the BES III Collaboration, since they provide the most precise measurements of the D_s^+ decays.

To collect the signal of $D_s^+ \rightarrow \ell^+ \nu_\ell$, it is useful to adopt the missing-squared-mass cut, which is defined as

$$M_{\text{miss}}^2 = E_{\text{miss}}^2 - \left| \vec{0} - \vec{p}_{\text{tag}} - \vec{p}_{\gamma(\pi^0)} - \vec{p}_\mu \right|^2, \quad (4.2)$$

with

$$E_{\text{miss}} = E_{\text{cm}} - E_{\text{tag}} - E_{\gamma(\pi^0)} - E_\mu, \quad (4.3)$$

where $\gamma(\pi^0)$ represents a monochromatic photon from $D_s^{*+} \rightarrow D_s^+ \gamma$ and two photons from $D_s^{*+} \rightarrow D_s^+ \pi^0 \rightarrow D_s^+ \gamma\gamma$. M_{miss}^2 is Lorentz invariant, while the RHS is defined in the laboratory frame.

In the $\ell = \mu$ channel, if there are no soft-photon radiations, this reduces to the invariant mass of a single neutrino and therefore must vanish, *i.e.*, $M_{\text{miss}}^2 = m_{\nu_\mu}^2 = 0$. The relation between the missing-squared-mass and the single soft-photon momentum in the D_s^+ rest frame is [38]

$$\begin{aligned} M_{\text{miss}}^2 &= (p_{\nu_\mu} + p_\gamma)^2 \\ &= 2E_{\nu_\mu} E_\gamma (1 - \cos \theta_{\nu\gamma}), \end{aligned} \quad (4.4)$$

where $\theta_{\nu\gamma}$ is an undetectable angle between emitted soft-photon and ν_μ . In the BES III experiments, to avoid a peaking background from $D_s^+ \rightarrow K_0\pi^+$ with missing K_0 , a hard cut $M_{\text{miss}}^2 < 0.2 \text{ GeV}^2$ has been set [74],^{#10} which leads to

$$E_\gamma E_{\nu_\mu} (1 - \cos \theta_{\nu\gamma}) < 0.1 \text{ GeV}^2. \quad (4.6)$$

In the soft-photon limit, the energy of the muon-neutrino is

$$E_{\nu_\mu} = \frac{m_{D_s}}{2} \left(1 - \frac{m_\mu^2}{m_{D_s}^2} \right) \quad \text{for } E_\gamma = 0. \quad (4.7)$$

For evaluation of magnitude of $\cos \theta_{\nu\gamma}$, we consider its expected value. Using the soft-photon approximation, the phase space integration is proportional to (see Eq. (3.10))

$$I = \int \frac{d^3\mathbf{k}}{(2\pi)^3} \frac{1}{2E_\gamma} \left[\frac{2p_{D_s} \cdot p_\ell}{(p_{D_s} \cdot k)(p_\ell \cdot k)} - \frac{m_{D_s}^2}{(p_{D_s} \cdot k)^2} - \frac{m_\ell^2}{(p_\ell \cdot k)^2} \right]. \quad (4.8)$$

Exploiting the fact that the lepton and neutrino are emitted almost back to back for the soft-photon process, we use $(\pi - \theta_{\nu\gamma})$ for the angle between the lepton and soft-photon. Then, the integral can be simplified to

$$I \propto \int d\Omega \left[\frac{2}{1 + \beta_\ell \cos \theta_{\nu\gamma}} - 1 - \frac{1 - \beta_\ell^2}{(1 + \beta_\ell \cos \theta_{\nu\gamma})^2} \right], \quad (4.9)$$

with

$$\beta_\ell = \frac{1 - x_\ell}{1 + x_\ell}. \quad (4.10)$$

This solid-angle integrand gives the (unnormalized) probability density function of the parameter $\theta_{\nu\gamma}$:

$$P(\theta_{\nu\gamma}) = \frac{2}{1 + \beta_\ell \cos \theta_{\nu\gamma}} - 1 - \frac{1 - \beta_\ell^2}{(1 + \beta_\ell \cos \theta_{\nu\gamma})^2}. \quad (4.11)$$

In Fig. 9, we show the $P(\theta_{\nu\gamma})$ for the μ and τ modes. From the probability density functions, we obtain the expected values:

$$\begin{aligned} \langle \cos \theta_{\nu\gamma} \rangle &= -0.8981 & \text{for } \mu \text{ mode}, \\ \langle \cos \theta_{\nu\gamma} \rangle &= -0.0511 & \text{for } \tau \text{ mode}. \end{aligned} \quad (4.12)$$

It clearly presents that in the μ mode, the soft photon tends to be emitted in the direction of the muon, whereas in the τ mode, it tends to be emitted in a direction different from that of the tau-neutrino and tau.

^{#10}The real photon radiations from $D_s^+ \rightarrow \mu^+ \nu_\mu$ do not affect another hard cut,

$$\Delta E \in (-0.05, 0.10) \text{ GeV}, \quad (4.5)$$

where $\Delta E = E_{\text{cm}} - E_{\text{tag}} - E_{\gamma(\pi^0)} - \sqrt{m_{D_s}^2 + |\vec{0} - \vec{p}_{\text{tag}} - \vec{p}_{\gamma(\pi^0)}|^2}$ [75]. Here, $\sqrt{m_{D_s}^2 + |\vec{p}_{\text{tag}} + \vec{p}_{\gamma(\pi^0)}|^2}$ corresponds to the energy of D_s^+ immediately after the production prior to the soft-photon emissions, so that the soft photons from the D_s^+ decays do not change ΔE .

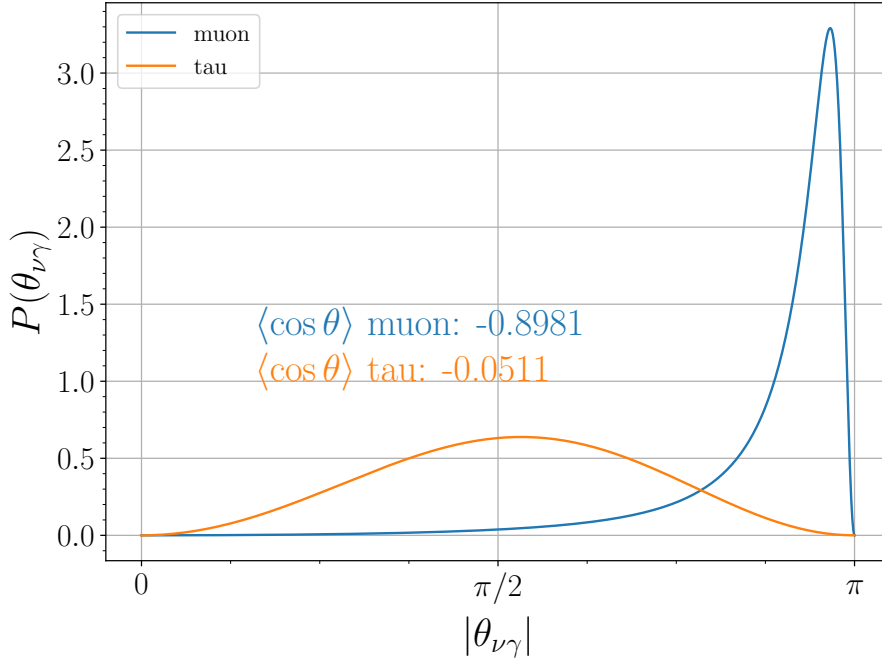


Figure 9: Probability density function of angle between the neutrino and soft photon.

Using Eqs. (4.7) and (4.12), for the μ mode we obtain a numerical expected value of E_{\max} as

$$E_{\gamma} < E_{\max} \simeq 54 \text{ MeV} \quad (\text{for } \mu \text{ mode}). \quad (4.13)$$

Note that this E_{\max} is calculated in the D_s^+ rest frame, which is precisely consistent with what we discussed in Sec. 3 for the long-distance QED corrections.

On the other hand, for the τ mode, the estimation of E_{\max} is more involved, because the invisible system has to consist of at least tau-neutrino, its anti-neutrino and possibly another neutrino, and the simple relation in Eq. (4.4) no longer holds. Furthermore, the cuts are entirely different depending on the τ^+ decay channels [76–80].

The most precise measurement is given via the $\tau^+ \rightarrow e^+ \nu_e \bar{\nu}_{\tau}$ channel for the τ decays [77]. In this measurement, the signals are tagged in an almost inclusive way with respect to soft photons,^{#11} excluding within a 5° cone of the positron direction. The second most precise measurement is given by $\tau^+ \rightarrow \pi^+ \bar{\nu}_{\tau}$ channel with the hard cut $M_{\text{miss}}^2 < 0.6 \text{ GeV}^2$ [80]. In this case, we expect

$$\begin{aligned} M_{\text{miss}}^2 &= (p_{\nu_{\tau}} + p_{\nu_{\bar{\tau}}} + p_{\gamma})^2 \\ &\simeq 2E_{\nu_{\bar{\tau}}} (E_{\gamma} + E_{\nu_{\tau}}). \end{aligned} \quad (4.14)$$

^{#11}Here, events with an extra electromagnetic-calorimeter-shower energy smaller than 0.4 GeV are selected. This is a less stringent cut compared to the maximum value of E_{γ} : $(m_{D_s}/2)(1 - m_{\tau}^2/m_{D_s}^2) = 182 \text{ MeV}$.

Here, a flat angular distribution is assumed for the soft-photon direction according to Fig. 9. Very naively, $2E_{\nu_{\bar{\tau}}} \simeq m_{\tau}$ holds because $\tau^+ \rightarrow \pi^+ \bar{\nu}_{\tau}$ is two-body decay. These relations give

$$E_{\gamma} + E_{\nu_{\tau}} \lesssim 340 \text{ MeV}. \quad (4.15)$$

Since this cut is less stringent than the maximum soft-photon energy $E_{\gamma} < 182 \text{ MeV}$, we conclude that this channel is also collected inclusively. Note that E_{max} dependence is very weak in the long-distance QED corrections for the τ mode, which will be shown in Sec. 4.3.

4.2 PHOTOS QED corrections

In many collider experiments, including BESIII, the PHOTOS Monte-Carlo generator has been used for the simulation of modifications of the kinematic variables induced by the FSR in the leading-logarithmic approximation [89–92]. It can be applied in a model-independent way even when the underlying amplitudes are not known, whereas the theoretical calculations are performed using the specific amplitudes derived from the (effective) models. Because some experimental results have already been corrected using the PHOTOS, the theoretical prediction has to be adjusted accordingly when assessing the precise impact of the QED corrections. In particular, one has to subtract the FSR contribution from the charged-lepton leg in the $D_s^+ \rightarrow \ell^+ \nu_{\ell}$ process.

The FSR contribution in the leading-logarithmic approximation comes from the soft-photon emission amplitude

$$i\mathcal{M}_0 e \frac{p_{\ell} \cdot \epsilon^*(k)}{p_{\ell} \cdot k + i\epsilon}, \quad (4.16)$$

with the self-energy correction

$$\left. \frac{d\Sigma}{d\phi} \right|_{\phi=m_{\ell}, \text{IR-div}} = -\frac{\alpha_0}{2\pi} \ln \frac{m_{\gamma}^2}{m_{\ell}^2}. \quad (4.17)$$

Then one finds the PHOTOS contribution

$$F^{\text{PHOTOS}} = \frac{\alpha_0}{2\pi} \left(-2 \ln \frac{2E_{\text{max}}}{m_{\ell}} - \frac{1+x_{\ell}}{1-x_{\ell}} \ln x_{\ell} \right), \quad (4.18)$$

which should be subtracted in the theoretical calculation of $\Gamma(D_s^+ \rightarrow \ell^+ \nu_{\ell})^{\text{LD}}$.

4.3 Numerical effects to $|V_{cs}|$ and CKM unitarity

In this section, we investigate the numerical impacts of the QED corrections to $D_s^+ \rightarrow \ell^+ \nu$ and extract the state-of-the-art value of $|V_{cs}|$ from the latest data. We also assess how the test of CKM unitarity is affected by the QED corrections.

First, we compare the magnitudes of the individual QED corrections to $\Gamma(D_s^+ \rightarrow \ell^+ \nu_{\ell})$ and show them in Fig. 10, as a function of E_{max} . The upper (lower) panel corresponds to the μ (τ) mode. The short-distance corrections are defined by $\delta^{\text{SD}} = \eta_{\text{EW}}^2 - 1$ and shown by the red-solid and red-dashed lines for the NDR and HV schemes, respectively. The long-distance corrections are decomposed as $\delta^{\text{LD}} = F^{\text{ISR}} + F^{\text{FSR}} + F^{\text{INT}} + F^{\text{hard}} + H^{(\text{a})} + H^{(\text{b+c})}$,

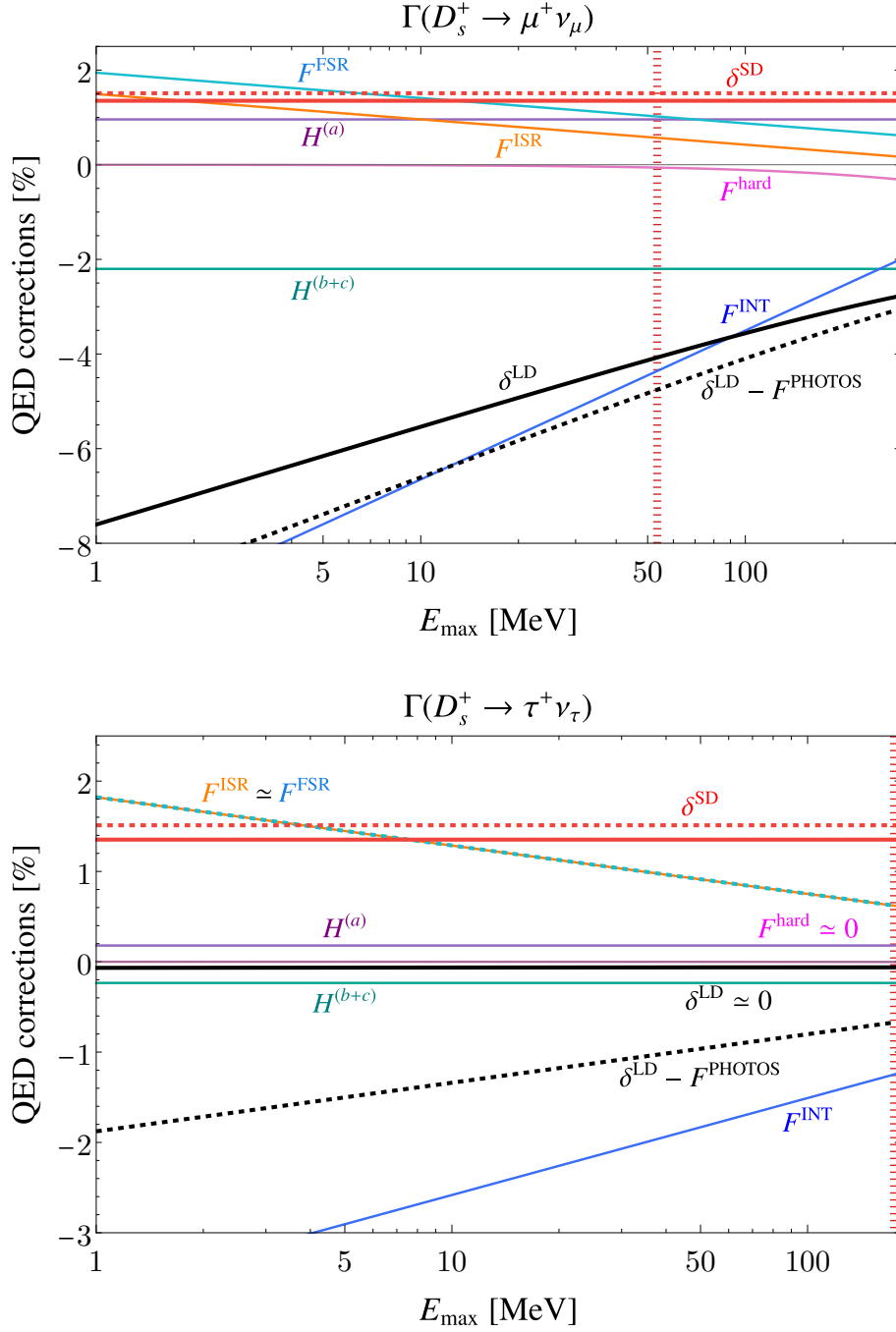


Figure 10: Each magnitude of the QED corrections to the decay rates of $D_s^+ \rightarrow \mu^+ \nu_\mu$ (upper panel) and $D_s^+ \rightarrow \tau^+ \nu_\tau$ (lower panel). Here, $\mu = 1 \text{ GeV}$ is taken for the long-distance virtual corrections. The short- and full long-distance corrections are shown by the red and black solid lines, respectively. The estimated E_{max} in the BESIII experiments is shown by the vertical red dotted lines. For a detailed explanation, see the main text.

see Eq. (3.20). For the virtual corrections $H^{(a)}$ and $H^{(b+c)}$, we take $\mu = 1$ GeV. The black-solid lines stand for the full long-distance QED corrections, while the black-dashed line represents the long-distance corrections after subtracting the PHOTOS QED correction in Eq. (4.18). The estimated E_{\max} in the BESIII experiments is shown by the vertical red dotted lines. For τ mode, the collected data are dominated by the soft-photon inclusive signals, see discussions in Sec. 4.1.

For μ mode, it is clearly shown that all of QED corrections (except for F^{hard}) are $\mathcal{O}(1)\%$ size and exceed the naive expected magnitude $\mathcal{O}(\alpha/\pi) \approx 0.2\%$. The total QED correction is dominated by the interference contributions (F^{INT}) between the ISR and FSR. Furthermore, it is partially canceled by the short-distance correction.

For τ mode, since the emitted τ is non-relativistic, all QED corrections are suppressed than the μ mode. Due to $m_\tau \sim m_{D_s}$ we find $F^{\text{ISR}} \simeq F^{\text{FSR}}$ and $F^{\text{ISR}} + F^{\text{FSR}} + F^{\text{INT}} \simeq 0$, and the full long-distance QED correction becomes consistent with the naive size $\mathcal{O}(\alpha/\pi)$. However, since the simulation by the PHOTOS takes into account only the contribution from the final state radiations, it implies that the simulations would lead to an overestimation of the QED correction, which comes out as the black dashed line ($\delta^{\text{LD}} - F^{\text{PHOTOS}}$) in the figure. Fortunately, we find that this overestimation is partially canceled by the short-distance correction.

Next, we extract the CKM component $|V_{cs}|$ from the latest data using the complete QED correction, subtracting the PHOTOS correction. The master formula for the extracted $|V_{cs}|$ in the NDR scheme is

$$|V_{cs}|^2 = \frac{\mathcal{B}(D_s^+ \rightarrow \ell^+ \nu_\ell)}{\tau_{D_s}} \left(\frac{G_F^2}{8\pi} m_{D_s} m_\ell^2 f_{D_s}^2 (1 - x_\ell)^2 \left\{ 1 + \frac{\alpha(m_{D_s})}{2\pi} \left[\ln \left(\frac{M_Z^2}{m_{D_s}^2} \right) + \frac{1}{2} \mathcal{A}_{g_s} - \frac{11}{6} \right] \right\}^2 \right. \\ \times \Omega_B \left(\Omega_B^{\text{PHOTOS}} \right)^{-1} \left\{ 1 + \frac{\alpha_0}{2\pi} \left[-2 - \frac{1+x_\ell}{1-x_\ell} \left(\frac{1}{2} \ln^2 x_\ell + 2 \text{Li}_2(1-x_\ell) \right) \right. \right. \\ \left. \left. - \frac{3}{2} \ln \frac{\mu^2}{m_{D_s} m_\ell} - \frac{1+15x_\ell}{4(1-x_\ell)} \ln x_\ell \right] + F^{\text{hard}} + \frac{\alpha_0}{2\pi} \frac{1+x_\ell}{1-x_\ell} \ln x_\ell \right\}^{-1} \right), \quad (4.19)$$

with the PHOTOS resummation factor

$$\Omega_B^{\text{PHOTOS}} = \left(\frac{2E_{\max}}{m_\ell} \right)^{-\frac{\alpha_0}{\pi}}. \quad (4.20)$$

For the latest data, we use the updated world averages from the 2025 update of the Review of Particle Physics by PDG [44],

$$\begin{aligned} \mathcal{B}(D_s^+ \rightarrow \mu^+ \nu_\mu) &= (5.37 \pm 0.11) \times 10^{-3}, \\ \mathcal{B}(D_s^+ \rightarrow \tau^+ \nu_\tau) &= (5.39 \pm 0.09) \times 10^{-2}, \end{aligned} \quad (4.21)$$

with $\tau_{D_s} = (5.012 \pm 0.022) \times 10^{-13}$ s.^{#12}

^{#12}The 2024 published edition of the PDG provides $\mathcal{B}(D_s^+ \rightarrow \mu^+ \nu_\mu) = (5.35 \pm 0.12) \times 10^{-3}$ and $\mathcal{B}(D_s^+ \rightarrow \tau^+ \nu_\tau) = (5.36 \pm 0.10) \times 10^{-2}$ [44].

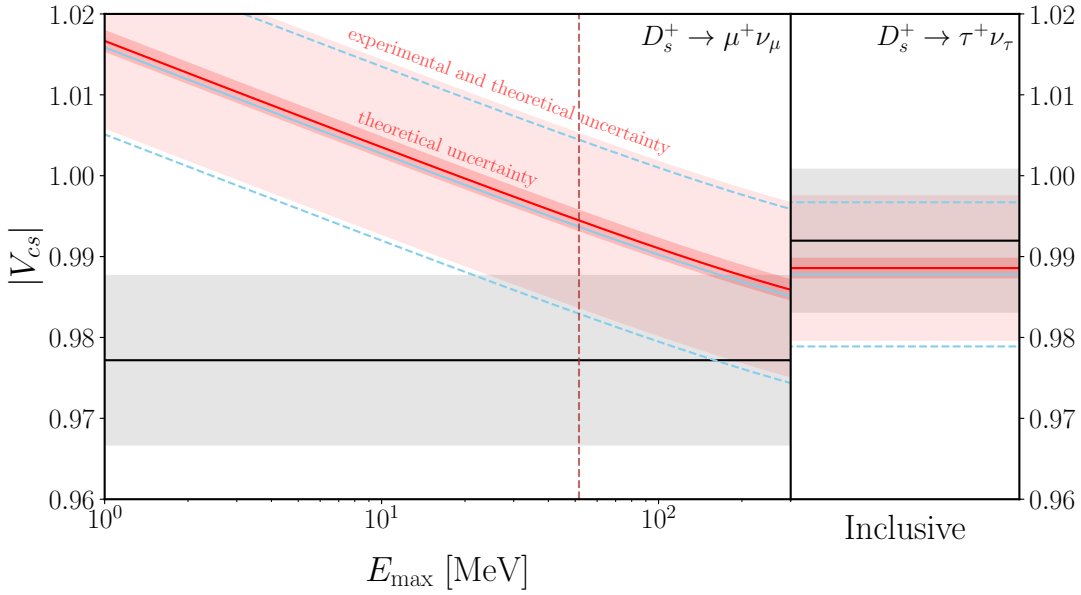


Figure 11: Extracted values of $|V_{cs}|$ from the latest data on D_s^+ leptonic decays in the μ (left panel), shown as a function of E_{\max} , and τ channels (right panel). The complete QED corrections evaluated in the NDR scheme are included in the red bands, while the gray bands show results obtained without any radiative corrections. The darker bands indicate the theoretical uncertainty from the long-distance QED corrections, evaluated by varying the renormalization scale $500 \text{ MeV} < \mu < 2 \text{ GeV}$ (the solid lines correspond to $\mu = 1 \text{ GeV}$). The lighter bands additionally incorporate the current experimental uncertainties. The light blue (dashed) lines show the results in the HV scheme.

The extracted values of $|V_{cs}|$ in each decay mode are shown in Fig. 11. The red bands include the complete QED corrections evaluated in the NDR scheme, while the gray bands do not include any radiative corrections. The theoretical uncertainty from the renormalization scale in the long-distance corrections is shown by the darker bands varying $500 \text{ MeV} < \mu < 2 \text{ GeV}$. The lighter bands additionally incorporate the experimental uncertainties. The light blue (dashed) lines show the results in the HV scheme. Hence, both the theoretical uncertainty and the regularization-scheme dependence are much smaller than the current sizable experimental uncertainty. This difference between the two schemes is incorporated as the theoretical uncertainty in the final result of $|V_{cs}|$ (next figure).

In addition, we evaluate the global fit of $|V_{cs}|$ incorporating the QED corrections. It is known that the most precise determination of $|V_{cs}|$ comes from D -meson semi-leptonic decay measurements: $D^0 \rightarrow K^- \ell^+ \nu_\ell$ and $D^+ \rightarrow \bar{K}^0 \ell^+ \nu_\ell$ ($\ell = e, \mu$). In Fig. 12, we summarize the extracted values of $|V_{cs}|$ from leptonic and semi-leptonic decays and those fitted values. The D -meson semi-leptonic decays are carefully studied in Ref. [36]. Here, we quote the “nominal” scenario of Ref. [36], in which the $D \rightarrow \bar{K}$ form factors utilizes the lattice results obtained by the HPQCD [93] and FNAL/MILC collaborations [94], then

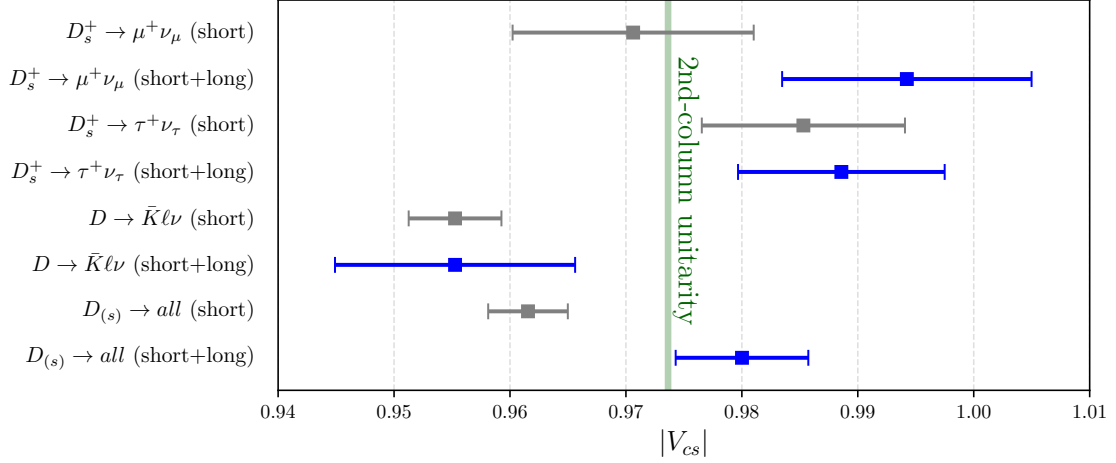


Figure 12: Summary of the determination of $|V_{cs}|$ from D_s^+ leptonic and D semi-leptonic decays. The gray bars include only short-distance corrections, while the blue bars further include the long-distance QED corrections. The green band represents the prediction of the CKM unitarity test from $(V^\dagger V)_{22}$.

we rescale it by obtaining short-distance correction in Eq. (2.25) in the NDR scheme. All gray bars indicate the results incorporating only short-distance corrections, while the blue bars include the long-distance QED corrections in D_s^+ -meson leptonic decays. Note that calculations of the long-distance QED corrections in D -meson semi-leptonic decays are currently missing. Following Refs. [19, 94], we add 1% uncertainty due to the missing long-distance QED corrections. From another point of view, the CKM unitarity predicts the green shaded region using the PDG average values of $|V_{us}|$ and $|V_{ts}|$ [44].

In Ref. [36], it was shown that when one considers the joint fit of $|V_{cs}|$ incorporating only short-distance corrections, then the CKM unitarity is significantly violated, which is clearly shown in this figure. On the other hand, we find that the long-distance QED corrections reduce the tension in the CKM unitarity test.

Finally, we numerically compare the fitted values of $|V_{cs}|$ with the CKM unitarity. First, the extracted values of $|V_{cs}|$ from $D_s^+ \rightarrow \mu^+ \nu_\mu$ and $D_s^+ \rightarrow \tau^+ \nu_\tau$ are

$$|V_{cs}|_{D_s \rightarrow \mu \nu} = 0.9942 \pm 0.0020_{\text{lat.}} \pm 0.0015_{\text{th.}} \pm 0.0105_{\text{exp.}}, \quad (4.22)$$

$$|V_{cs}|_{D_s \rightarrow \tau \nu} = 0.9886 \pm 0.0020_{\text{lat.}} \pm 0.0014_{\text{th.}} \pm 0.0086_{\text{exp.}}, \quad (4.23)$$

respectively, where the theoretical uncertainty comes from the renormalization group scale dependence $500 \text{ MeV} < \mu < 2 \text{ GeV}$ and the regularization-scheme dependence, while the experimental uncertainty is dominated by the branching ratios in Eq. (4.21). Combining the two channels, we obtain

$$|V_{cs}|_{D_s} = 0.991 \pm 0.007. \quad (4.24)$$

Table 1: Results of the second-column CKM unitarity test. For $D \rightarrow \bar{K}\ell\nu$, only the short-distance corrections (NDR) are taken into account, while its second uncertainties come from an estimation of the size of missing long-distance QED corrections.

scenario	data set	$ V_{cs} $	Δ_{CKM}	result
nominal	$D \rightarrow \bar{K}\ell\nu$	$0.955 \pm 0.004 \pm 0.010$	0.012 ± 0.011	1.1σ
	all average	0.980 ± 0.006		
scale factor	$D \rightarrow \bar{K}\ell\nu$	$0.959 \pm 0.007 \pm 0.010$	0.018 ± 0.012	1.6σ
	all average	0.983 ± 0.006		

Furthermore, combining it with the D semi-leptonic decay measurements which are summarized in Table 1, we obtain the fitted value of $|V_{cs}|$

$$|V_{cs}| = \begin{cases} 0.980 \pm 0.006 & (\text{nominal}), \\ 0.983 \pm 0.006 & (\text{scale factor}), \end{cases} \quad (4.25)$$

where the “scale factor” scenario is defined in Ref. [36]: For the $D \rightarrow \bar{K}$ form factors, in addition to the HPQCD and FNAL/MILC, the lattice results obtained by the ETM collaboration [95, 96] is also used. However, it is known that the ETM results are not mutually consistent with those of HPQCD and FNAL/MILC. Hence, including the ETM results leads to an additional scale factor in the systematic uncertainty. As a result, the fitted result for D semi-leptonic decays in the scale-factor scenario has a larger uncertainty.

Now, let us check the unitarity of the CKM matrix using $|V_{cs}|$ obtained in Eq. (4.25). In Ref. [36], it is reported that both the second-row and second-column unitarity conditions exhibit a significant deficit when only the short-distance corrections are taken into account. For the second-row unitarity test, the CKM component $|V_{cd}|$ must also be determined from data, including QED radiative corrections. However, these studies are currently missing the calculation of the QED corrections [19], and $|V_{cd}|$ is also determined from the neutrino scattering data [44]. On the other hand, there have been many efforts to calculate the QED corrections to $|V_{us}|$, so that we focus on the second-column CKM unitarity test,

$$(V^\dagger V)_{22} = |V_{us}|^2 + |V_{cs}|^2 + |V_{ts}|^2 = 1. \quad (4.26)$$

The measure of the CKM unitarity violation is represented by Δ_{CKM} , defined as

$$\Delta_{\text{CKM}} \equiv |V_{us}|^2 + |V_{cs}|^2 + |V_{ts}|^2 - 1. \quad (4.27)$$

By using the world averages of $|V_{us}|$ and $|V_{ts}|$ by the PDG [44]

$$|V_{us}| = 0.22431 \pm 0.00085, \quad (4.28)$$

$$|V_{ts}| = (41.5 \pm 0.9) \times 10^{-3}, \quad (4.29)$$

we conclude

$$\Delta_{\text{CKM}} = \begin{cases} 0.012 \pm 0.011 & (\text{nominal}), \\ 0.018 \pm 0.012 & (\text{scale factor}), \end{cases} \quad (4.30)$$

which are consistent with the CKM unitarity condition at 1.1σ and 1.6σ levels, respectively. Furthermore, even if we use the result by a global fit of $|V_{us}| = 0.22405 \pm 0.00035$ in Ref. [6], we obtain the same values of Δ_{CKM} for both scenarios. These results are summarized in Table 1.

It is found that, in the nominal scenario, the second-column CKM unitarity condition is well satisfied. We hope that, once the long-distance QED corrections to $D \rightarrow \bar{K}\ell\nu$ are taken into account, the CKM unitarity will be more robustly checked in future studies, as expected from Fig. 12.

5 Discussion and Conclusions

In this article, we carefully studied the short-distance EW-QED corrections and the long-distance QED corrections to $D_s^+ \rightarrow \ell^+\nu_\ell$ decays at one-loop level within the SM. We analytically confirmed two minor contributions which are often neglected in previous phenomenological analyses; (1) the non-logarithm correction in the short-distance correction and (2) the correction from the non-soft-photon radiation corresponds to $\mathcal{O}(E_{\text{max}})$ contribution. On the other hand, for the first time, the radiative corrections were calculated in both the NDR and HV schemes, and the theoretical uncertainty arising from the regularization-scheme difference was considered.

We found that properly including these radiative corrections is essential to bring the second-column CKM unitarity tests into agreement with the SM prediction. Our study highlights that the present bottleneck in confirming CKM unitarity is the precision of the QED corrections. This underscores the importance of further improving lattice simulations by consistently incorporating QED effects to achieve more stringent and reliable tests of CKM unitarity.

In this work, the structure-dependent QED corrections are not included. Recently, the structure-dependent QED corrections to $B^+ \rightarrow \ell^+\nu$ were calculated by using a gauge invariant formalism [97]. It was found that the *virtual* structure-dependent corrections are non-negligible in $B^+ \rightarrow \ell^+\nu$, which partially cancels the long-distance QED corrections evaluated by the scalar QED. However, both the size and sign of the virtual structure-dependent QED corrections are not clear a priori in $D_s^+ \rightarrow \ell^+\nu$, because the QED charges of the quark lines are different and the directions of the internal fermion lines in the loop differ from the B^+ decays. (The size is expected to be mildly suppressed compared to the ones in $B^+ \rightarrow \ell^+\nu$ by replacement of $m_B \rightarrow m_{D_s}, m_b \rightarrow m_c$.) Therefore, we leave the investigation of these effects in both $D_s^+ \rightarrow \ell^+\nu$ and $D \rightarrow \bar{K}\ell^+\nu$ to future work.

Acknowledgments

We are profoundly grateful to Toru Goto for sharing his calculation notes with us, carefully checking our results, and providing many insightful comments. We would like to thank Huijing Li, Rong-Gang Ping, and Jin Min Yang for valuable discussions on the D_s^+ -meson measurements in the BESIII experiment. We also thank Motoi Endo and Takashi

Kaneko for useful discussions. The work of T.K. is supported by the JSPS Grant-in-Aid for Scientific Research Grant No. 24K22872 and 25K07276.

A Details of the short-distance corrections

A.1 Regularization scheme dependence

We use dimensional regularization to handle the UV divergence. There are two regularization schemes: the naive dimensional regularization (NDR) and the 't Hooft-Veltman scheme (HV, also BMHV), which depend on how γ_5 is treated. One-loop four-Fermi operators have the following structures inserted four gamma matrices in the tree-level operator: $[\psi\Gamma\psi][\psi\Gamma\psi] \equiv \Gamma \otimes \Gamma$ with $\Gamma = \gamma^\nu(1 - \gamma_5)/2$. Contractions of these operators give [49]

$$\begin{aligned}\gamma_\mu\gamma_\rho\Gamma\gamma^\rho\gamma^\mu\otimes\Gamma &= A_1(\epsilon)\Gamma\otimes\Gamma + E_1, \\ \Gamma\gamma_\mu\gamma_\rho\otimes\Gamma\gamma^\mu\gamma^\rho &= A_2(\epsilon)\Gamma\otimes\Gamma + E_2, \\ \Gamma\gamma_\mu\gamma_\rho\otimes\gamma^\rho\gamma^\mu\Gamma &= A_3(\epsilon)\Gamma\otimes\Gamma + E_3,\end{aligned}\tag{A.1}$$

where A_i are given as

$$A_1(\epsilon) = A_3(\epsilon) = \begin{cases} 4(1 - \epsilon)^2 & (\text{NDR}), \\ 4(1 + \epsilon^2) & (\text{HV}), \end{cases}\tag{A.2}$$

and

$$A_2(\epsilon) = 4(4 - \epsilon - \epsilon^2) \quad (\text{NDR, HV}).\tag{A.3}$$

The extra term E_i is the scheme-dependent evanescent operator.

A.2 Matching onto the weak Hamiltonian

In this section, we describe the details of the calculations of the γW -box diagrams. By calculating the one-loop box diagrams in Fig. 1, we obtain

$$\begin{aligned}i\mathcal{M}_{(a)}^{\gamma W} &= i\mathcal{M}_0 Q_s Q_\ell \\ &\times \frac{\alpha}{\pi} \left\{ \underbrace{\frac{3}{8} + \frac{1}{4} \ln \left[\frac{2M_W^2}{s(1 - \cos \theta)} \right]}_{\ell^2} - \underbrace{\frac{\pi^2}{6} - \frac{1}{4} \ln^2 \left[\frac{2m_\gamma^2}{s(1 - \cos \theta)} \right] - \ln \left[\frac{2m_\gamma^2}{s(1 - \cos \theta)} \right] - \frac{5}{4}}_{\ell^0} \right\},\end{aligned}\tag{A.4}$$

$$\begin{aligned}i\mathcal{M}_{(d)}^{\gamma W} &= i\mathcal{M}_0 Q_c Q_\ell \\ &\times \frac{\alpha}{\pi} \left\{ \underbrace{-\frac{3}{2} - \ln \left[\frac{2M_W^2}{s(1 + \cos \theta)} \right]}_{\ell^2} + \underbrace{\frac{\pi^2}{6} + \frac{1}{4} \ln^2 \left[\frac{2m_\gamma^2}{s(1 + \cos \theta)} \right] + \ln \left[\frac{2m_\gamma^2}{s(1 + \cos \theta)} \right] + \frac{3}{2}}_{\ell^0} \right\},\end{aligned}\tag{A.5}$$

for the terms proportional to ℓ^2 and ℓ^0 in the numerators of the loop calculations, respectively, where ℓ denotes the loop momentum.

By calculating the virtual γ corrections in Fig. 2 to the matching onto the weak Hamiltonian, we obtain

$$i\mathcal{M}_{(a)}^\gamma = i\mathcal{M}_0 Q_s Q_\ell \times \frac{\alpha}{\pi} \left\{ \underbrace{\frac{1}{4\bar{\epsilon}} + \frac{1}{4} + \frac{1}{4} \ln \left[\frac{2\mu^2}{s(1-\cos\theta)} \right]}_{\ell^2} - \underbrace{\frac{\pi^2}{6} - \frac{1}{4} \ln^2 \left[\frac{2m_\gamma^2}{s(1-\cos\theta)} \right] - \ln \left[\frac{2m_\gamma^2}{s(1-\cos\theta)} \right] - \frac{5}{4}}_{\ell^0} \right\}, \quad (\text{A.6})$$

$$i\mathcal{M}_{(b)}^\gamma = i\mathcal{M}_0 Q_c Q_\ell \times \frac{\alpha}{\pi} \left\{ \underbrace{-\frac{1}{\bar{\epsilon}} - \frac{11}{4} - \ln \left[\frac{2\mu^2}{s(1+\cos\theta)} \right]}_{\ell^2} + \underbrace{\frac{\pi^2}{6} + \frac{1}{4} \ln^2 \left[\frac{2m_\gamma^2}{s(1+\cos\theta)} \right] + \ln \left[\frac{2m_\gamma^2}{s(1+\cos\theta)} \right] + \frac{3}{2}}_{\ell^0} \right\}. \quad (\text{A.7})$$

One can find that l^0 contributions from both box and four-Fermi diagrams are entirely identical in each diagram: the IR divergences, angular dependence, and s dependence are totally canceled in Eqs. (2.13) and (2.14).

B Details of the long-distance corrections

B.1 Lagrangian

Below the EW energy scale, the effective Lagrangian that explains $D_s^+ \rightarrow \ell^+ \nu_\ell$ is

$$\mathcal{L}_{c\bar{s} \rightarrow \ell^+ \nu} = -\frac{G_F}{\sqrt{2}} V_{cs}^* [\bar{\nu}_\ell \gamma^\mu (1 - \gamma_5) \ell] [\bar{s} \gamma_\mu (1 - \gamma_5) c]. \quad (\text{B.1})$$

The tree-level decay amplitude can be obtained by

$$\begin{aligned} i\mathcal{M}_0 &= -i \frac{G_F}{\sqrt{2}} V_{cs}^* \langle \ell^+ \nu_\ell | [\bar{\nu}_\ell \gamma^\mu (1 - \gamma_5) \ell] [\bar{s} \gamma_\mu (1 - \gamma_5) c] | D_s^+ \rangle \\ &= -i \frac{G_F}{\sqrt{2}} V_{cs}^* \bar{u}_{\nu_\ell} \gamma^\mu (1 - \gamma_5) v_\ell \langle 0 | \bar{s} \gamma_\mu (1 - \gamma_5) c | D_s^+ \rangle \\ &= i \frac{G_F}{\sqrt{2}} V_{cs}^* \bar{u}_{\nu_\ell} \gamma^\mu (1 - \gamma_5) v_\ell \langle 0 | \bar{s} \gamma_\mu \gamma_5 c | D_s^+ \rangle \\ &= -\frac{G_F}{\sqrt{2}} V_{cs}^* f_{D_s} \bar{u}_{\nu_\ell} \not{p}_{D_s} (1 - \gamma_5) v_\ell. \end{aligned} \quad (\text{B.2})$$

B.2 Dilogarithm formula

The following identity between four dilogarithm functions is used in the calculation of the long-distance QED corrections:

$$\text{Li}_2 \left(\frac{x}{1+x} \right) - \text{Li}_2 \left(\frac{1}{1+x} \right) + 4 \text{Li}_2 \left(\frac{1-x}{1+x} \right) - \text{Li}_2 \left[\left(\frac{1-x}{1+x} \right)^2 \right] = \ln x \ln(1+x) + 2 \text{Li}_2(1-x), \quad (\text{B.3})$$

which is valid for $x > 0$.

According to Ref. [86], the soft-photon emission from a meson can be written as

$$\frac{\Gamma(M \rightarrow \ell \nu \gamma_{\text{soft}})}{\Gamma(M \rightarrow \ell \nu)} = \frac{\alpha}{2\pi} \sum_{i,j=0}^1 Q_i Q_j \left[4b_{ij} \ln \left(\frac{m_\gamma}{2E_{\text{max}}} \right) + 2F_{ij} + \mathcal{O}(E_{\text{max}}) \right], \quad (\text{B.4})$$

where $Q_1 = Q_\ell$ and $Q_0 = -Q_\ell$. The functions of b_{ij} and F_{ij} are defined in Ref. [86].

The coefficient of the $\ln m_\gamma$ term can be expressed as

$$4(b_{00} + b_{11} - 2b_{01}) = 4 \left(1 + \frac{1+x_\ell}{2(1-x_\ell)} \ln x_\ell \right), \quad (\text{B.5})$$

where $x_\ell = m_\ell^2/m_{D_s}^2$. This coefficient is consistent with our result in Eq. (3.12).

Furthermore, the finite corrections F_{ij} can be expressed as

$$\begin{aligned} 2(F_{00} + F_{11} - 2F_{01}) &= 2 - \frac{1+x_\ell}{1-x_\ell} \ln x_\ell - \frac{1+x_\ell}{1-x_\ell} \left\{ \frac{1}{2} \ln^2 x_\ell - \ln x_\ell \ln(1+x_\ell) \right. \\ &\quad \left. + \text{Li}_2 \left(\frac{x_\ell}{1+x_\ell} \right) - \text{Li}_2 \left(\frac{1}{1+x_\ell} \right) + 4 \text{Li}_2 \left(\frac{1-x_\ell}{1+x_\ell} \right) - \text{Li}_2 \left[\left(\frac{1-x_\ell}{1+x_\ell} \right)^2 \right] \right\} \\ &= 2 - \frac{1+x_\ell}{1-x_\ell} \left[\ln x_\ell + \frac{1}{2} \ln^2 x_\ell + 2 \text{Li}_2(1-x_\ell) \right], \end{aligned} \quad (\text{B.6})$$

which is again consistent with our result in Eq. (3.12).

B.3 Photon energy cut

Soft photon approximation is valid for small photon energies, and if possible, it is desired not to use the approximation. Therefore, we introduced the following two photon energy cuts:

$$\begin{aligned} 0 &\leq E_\gamma < E_{\text{cut}} && (\text{for IR limit}), \\ E_{\text{cut}} &\leq E_\gamma \leq E_{\text{max}} && (\text{for 3-body decay}). \end{aligned} \quad (\text{B.7})$$

The IR limit is shown by the red point in Fig. 13, where we used the soft photon approximation and took the $E_{\text{cut}} \rightarrow 0$. In the remaining shaded area, we used the Dalitz plot integration. When one integrates the entire region surrounded by the gray line, it represents the inclusive limit.

B.4 Inclusive limit

The inner-bremsstrahlung ratio for the inclusive D_s^+ leptonic decay is

$$\begin{aligned} \frac{\Delta P_{\text{IB}}}{P_0} &= \frac{\alpha}{\pi} \left[2 \left(1 + \frac{1+x_\ell}{2(1-x_\ell)} \ln x_\ell \right) \left(\ln \frac{m_\gamma}{m_{D_s}} - \ln(1-x_\ell) - \frac{1}{4} \ln x_\ell + \frac{3}{4} \right) \right. \\ &\quad \left. - \frac{x_\ell(10-7x_\ell)}{4(1-x_\ell)^2} \ln x_\ell - \frac{2(1+x_\ell)}{1-x_\ell} \text{Li}_2(1-x_\ell) + \frac{15-21x_\ell}{8(1-x_\ell)} \right], \end{aligned} \quad (\text{B.8})$$

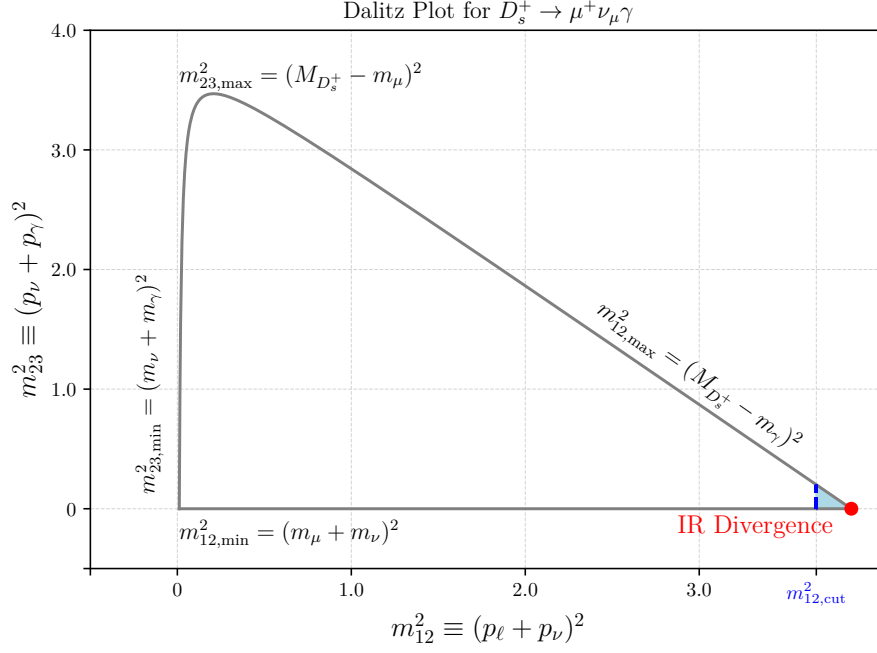


Figure 13: The Dalitz plot for $D_s^+ \rightarrow \mu\nu_\mu\gamma$ is shown in units of $[\text{GeV}^2]$. The entire region enclosed by the gray boundary corresponds to the inclusive limit, while the blue-shaded area represents the soft-photon region relevant to the present study. The cutoff value is given by $m_{12,\text{cut}}^2 = (p_\ell + p_\nu)^2 = (p_{D_s} - p_\gamma)^2 = m_{D_s}^2 - 2m_{D_s}E_{\text{max}}$, and the red point denotes the position at which the IR divergence appears, where the calculation has been performed using the soft-photon approximation in Eq. (3.11).

which is consistent with Eq. (4) of Ref. [87]. We numerically checked it and this is readily verified by plotting in Fig. 14, where the IR divergence is completely canceled by the following virtual corrections. The virtual photon vertex correction is

$$\frac{\Delta\Gamma_{\text{vert}}}{\Gamma_0} = \frac{\alpha}{2\pi} \left[-2 \left(\frac{1}{\epsilon} + \ln \frac{\mu^2}{m_{D_s}^2} \right) + \frac{1-3x_\ell}{1-x_\ell} \ln x_\ell - 2 - 2 \left(\frac{1+x_\ell}{1-x_\ell} \right) \ln x_\ell \ln \frac{m_\gamma}{\sqrt{m_{D_s}m_\ell}} \right], \quad (\text{B.9})$$

and the self-energy contribution is

$$\frac{\Delta\Gamma_{\text{self}}}{\Gamma_0} = \frac{\alpha}{2\pi} \left[\frac{1}{2} \left(\frac{1}{\epsilon} + \ln \frac{\mu^2}{m_{D_s}^2} \right) + \frac{1}{2} \ln \frac{m_\ell^2}{m_{D_s}^2} - 2 - 4 \ln \frac{m_\gamma}{\sqrt{m_{D_s}m_\ell}} \right]. \quad (\text{B.10})$$

References

- [1] M. Kobayashi and T. Maskawa, “CP Violation in the Renormalizable Theory of Weak Interaction,” *Prog. Theor. Phys.* **49** (1973) 652–657. (page 1).
- [2] B. Belfatto, R. Beradze, and Z. Berezhiani, “The CKM unitarity problem: A trace of new physics at the TeV scale?” *Eur. Phys. J. C* **80** (2020) 149 [arXiv:1906.02714]. (page 2).

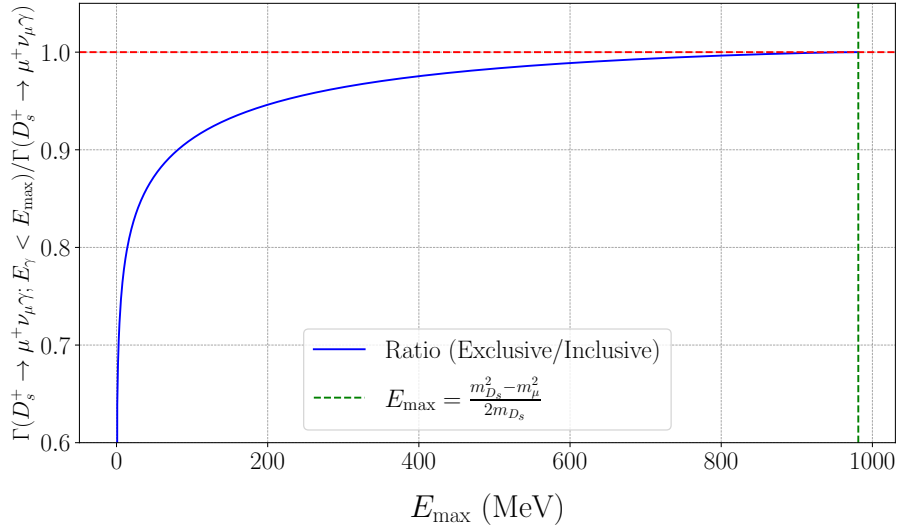


Figure 14: The ratio of the single photon radiation with $E_\gamma < E_{\max}$ in Eq. (3.12) to the inclusive one in Eq. (B.8) is indicated by the blue line. It equals to one at the $E_{\max} \rightarrow (m_{D_s}^2 - m_\mu^2)/2m_{D_s}$.

- [3] K. Cheung, W.-Y. Keung, C.-T. Lu, and P.-Y. Tseng, “Vector-like Quark Interpretation for the CKM Unitarity Violation, Excess in Higgs Signal Strength, and Bottom Quark Forward-Backward Asymmetry,” *JHEP* **05** (2020) 117 [[arXiv:2001.02853](#)].
- [4] B. Belfatto and Z. Berezhiani, “Are the CKM anomalies induced by vector-like quarks? Limits from flavor changing and Standard Model precision tests,” *JHEP* **10** (2021) 079 [[arXiv:2103.05549](#)].
- [5] G. C. Branco, J. T. Penedo, P. M. F. Pereira, M. N. Rebelo, and J. I. Silva-Marcos, “Addressing the CKM unitarity problem with a vector-like up quark,” *JHEP* **07** (2021) 099 [[arXiv:2103.13409](#)].
- [6] A. Crivellin, M. Kirk, T. Kitahara, and F. Mescia, “Global fit of modified quark couplings to EW gauge bosons and vector-like quarks in light of the Cabibbo angle anomaly,” *JHEP* **03** (2023) 234 [[arXiv:2212.06862](#)]. (pages 2, 27).
- [7] M. Endo and S. Mishima, “Muon $g - 2$ and CKM unitarity in extra lepton models,” *JHEP* **08** (2020) 004 [[arXiv:2005.03933](#)]. (page 2).
- [8] A. Crivellin, F. Kirk, C. A. Manzari, and M. Montull, “Global Electroweak Fit and Vector-Like Leptons in Light of the Cabibbo Angle Anomaly,” *JHEP* **12** (2020) 166 [[arXiv:2008.01113](#)].
- [9] M. Kirk, “Cabibbo anomaly versus electroweak precision tests: An exploration of extensions of the Standard Model,” *Phys. Rev. D* **103** (2021) 035004 [[arXiv:2008.03261](#)]. (page 2).
- [10] A. Hocker, H. Lacker, S. Laplace, and F. Le Diberder, “A New approach to a global fit of the CKM matrix,” *Eur. Phys. J. C* **21** (2001) 225–259 [[hep-ph/0104062](#)]. (page 2).
- [11] **CKMfitter Group** Collaboration, “CP violation and the CKM matrix: Assessing the

- impact of the asymmetric B factories,” *Eur. Phys. J. C* **41** (2005) 1–131 [[hep-ph/0406184](#)]. (page 2).
- [12] **UTfit** Collaboration, “The 2004 UTfit collaboration report on the status of the unitarity triangle in the standard model,” *JHEP* **07** (2005) 028 [[hep-ph/0501199](#)]. (page 2).
 - [13] **UTfit** Collaboration, “Model-independent constraints on $\Delta F = 2$ operators and the scale of new physics,” *JHEP* **03** (2008) 049 [[arXiv:0707.0636](#)]. (page 2).
 - [14] G. Buchalla and A. J. Buras, “ $K \rightarrow \pi \nu \bar{\nu}$ and high precision determinations of the CKM matrix,” *Phys. Rev. D* **54** (1996) 6782–6789 [[hep-ph/9607447](#)]. (pages 2, 11).
 - [15] A. J. Buras, M. Gorbahn, U. Haisch, and U. Nierste, “Charm quark contribution to $K^+ \rightarrow \pi^+ \nu \bar{\nu}$ at next-to-next-to-leading order,” *JHEP* **11** (2006) 002 [[hep-ph/0603079](#)]. [Erratum: *JHEP* 11, 167 (2012)].
 - [16] C. Lehner, E. Lunghi, and A. Soni, “Emerging lattice approach to the K-Unitarity Triangle,” *Phys. Lett. B* **759** (2016) 82–90 [[arXiv:1508.01801](#)].
 - [17] E. Lunghi and A. Soni, “Light quark loops in $K^\pm \rightarrow \pi^\pm \nu \bar{\nu}$ from vector meson dominance and update on the Kaon Unitarity Triangle,” *JHEP* **12** (2024) 097 [[arXiv:2408.11190](#)].
 - [18] A. Dery, “Natural complex plane for kaon CKM data: Framework, status, and future prospects,” *Phys. Rev. D* **112** (2025) 053005 [[arXiv:2504.12386](#)]. (page 2).
 - [19] **Flavour Lattice Averaging Group (FLAG)** Collaboration, “FLAG Review 2024,” [arXiv:2411.04268](#). (pages 2, 12, 25, 26).
 - [20] A. T. Yue, *et al.*, “Improved Determination of the Neutron Lifetime,” *Phys. Rev. Lett.* **111** (2013) 222501 [[arXiv:1309.2623](#)]. (page 2).
 - [21] T. Kitahara and K. Tobioka, “MeV sterile neutrino in light of the Cabibbo-angle anomaly,” *Phys. Rev. D* **108** (2023) 115034 [[arXiv:2308.13003](#)]. (page 2).
 - [22] P.-X. Ma, *et al.*, “Lattice QCD Calculation of Electroweak Box Contributions to Superaligned Nuclear and Neutron Beta Decays,” *Phys. Rev. Lett.* **132** (2024) 191901 [[arXiv:2308.16755](#)]. (page 2).
 - [23] F. Moretti, M. Gorbahn, and S. Jäger, “Beyond Leading Logarithms in g_V : The Semileptonic Weak Hamiltonian at $\mathcal{O}(\alpha \alpha_s^2)$,” [arXiv:2510.27648](#). (page 2).
 - [24] Z. Cao, R. J. Hill, R. Plestid, and P. Vander Griend, “The $Z\alpha^2$ correction to superallowed beta decays in effective field theory and implications for $|V_{ud}|$,” [arXiv:2511.05446](#).
 - [25] Ò. L. Crosas and E. Mereghetti, “Radiative corrections to superallowed beta decays at $\mathcal{O}(\alpha^2 Z)$,” [arXiv:2511.05481](#). (page 2).
 - [26] C.-Y. Seng and M. Gorchtein, “Electroweak nuclear radii constrain the isospin breaking correction to V_{ud} ,” *Phys. Lett. B* **838** (2023) 137654 [[arXiv:2208.03037](#)]. (page 2).
 - [27] C.-Y. Seng and M. Gorchtein, “Data-driven reevaluation of f_t values in superallowed β decays,” *Phys. Rev. C* **109** (2024) 045501 [[arXiv:2309.16893](#)].
 - [28] M. Gorchtein, V. Katyal, B. Ohayon, B. K. Sahoo, and C.-Y. Seng, “Cabibbo-Kobayashi-Maskawa unitarity deficit reduction via finite nuclear size,” *Phys. Rev. Res.* **7** (2025) L042002 [[arXiv:2502.17070](#)]. (page 2).
 - [29] Y. Grossman, E. Passemar, and S. Schacht, “On the Statistical Treatment of the Cabibbo Angle Anomaly,” *JHEP* **07** (2020) 068 [[arXiv:1911.07821](#)]. (page 2).

- [30] A. M. Coutinho, A. Crivellin, and C. A. Manzari, “Global Fit to Modified Neutrino Couplings and the Cabibbo-Angle Anomaly,” *Phys. Rev. Lett.* **125** (2020) 071802 [[arXiv:1912.08823](#)]. (page 2).
- [31] N. Carrasco, *et al.*, “QED Corrections to Hadronic Processes in Lattice QCD,” *Phys. Rev. D* **91** (2015) 074506 [[arXiv:1502.00257](#)]. (pages 2, 14).
- [32] V. Lubicz, *et al.*, “Finite-Volume QED Corrections to Decay Amplitudes in Lattice QCD,” *Phys. Rev. D* **95** (2017) 034504 [[arXiv:1611.08497](#)].
- [33] D. Giusti, *et al.*, “First lattice calculation of the QED corrections to leptonic decay rates,” *Phys. Rev. Lett.* **120** (2018) 072001 [[arXiv:1711.06537](#)].
- [34] M. Di Carlo, *et al.*, “Light-meson leptonic decay rates in lattice QCD+QED,” *Phys. Rev. D* **100** (2019) 034514 [[arXiv:1904.08731](#)].
- [35] R. Frezzotti, *et al.*, “Comparison of lattice QCD+QED predictions for radiative leptonic decays of light mesons with experimental data,” *Phys. Rev. D* **103** (2021) 053005 [[arXiv:2012.02120](#)]. (page 2).
- [36] C. Bognani, M. Reboud, D. van Dyk, and K. K. Vos, “Constraining $|V_{cs}|$ and physics beyond the Standard Model from exclusive (semi)leptonic charm decays,” *JHEP* **09** (2024) 099 [[arXiv:2407.06145](#)]. (pages 3, 24, 25, 26).
- [37] L. Wolfenstein, “Parametrization of the Kobayashi-Maskawa Matrix,” *Phys. Rev. Lett.* **51** (1983) 1945. (page 3).
- [38] S. de Boer, T. Kitahara, and I. Nisandzic, “Soft-Photon Corrections to $\bar{B} \rightarrow D\tau^-\bar{\nu}_\tau$ Relative to $\bar{B} \rightarrow D\mu^-\bar{\nu}_\mu$,” *Phys. Rev. Lett.* **120** (2018) 261804 [[arXiv:1803.05881](#)]. (pages 3, 17, 18).
- [39] A. J. Buras, “Weak Hamiltonian, CP violation and rare decays,” in *Les Houches Summer School in Theoretical Physics, Session 68: Probing the Standard Model of Particle Interactions*, pp. 281–539. 1998. [hep-ph/9806471](#). (pages 3, 7).
- [40] A. Sirlin, “Current Algebra Formulation of Radiative Corrections in Gauge Theories and the Universality of the Weak Interactions,” *Rev. Mod. Phys.* **50** (1978) 573. [Erratum: *Rev. Mod. Phys.* 50, 905 (1978)]. (pages 3, 10).
- [41] A. Sirlin, “Large m_W, m_Z Behavior of the $O(\alpha)$ Corrections to Semileptonic Processes Mediated by W ,” *Nucl. Phys. B* **196** (1982) 83–92. (pages 9, 11).
- [42] W. J. Marciano and A. Sirlin, “On Some General Properties of the $O(\alpha)$ Corrections to Parity Violation in Atoms,” *Phys. Rev. D* **29** (1984) 75. [Erratum: *Phys. Rev. D* 31, 213 (1985)].
- [43] W. J. Marciano and A. Sirlin, “Radiative Corrections to β Decay and the Possibility of a Fourth Generation,” *Phys. Rev. Lett.* **56** (1986) 22. (pages 3, 10, 11).
- [44] **Particle Data Group** Collaboration, “Review of particle physics,” *Phys. Rev. D* **110** (2024) 030001. and 2025 update available at the PDG website <https://pdg.lbl.gov>. (pages 4, 5, 8, 10, 14, 23, 25, 26).
- [45] J. Erler, “Calculation of the QED coupling $\hat{\alpha}(M_Z)$ in the modified minimal subtraction scheme,” *Phys. Rev. D* **59** (1999) 054008 [[hep-ph/9803453](#)]. (page 5).
- [46] A. Sirlin, “Radiative Corrections in the $SU(2)_L \times U(1)$ Theory: A Simple Renormalization Framework,” *Phys. Rev. D* **22** (1980) 971–981. (page 5).

- [47] R. G. Stuart, “General renormalization of the gauge invariant perturbation expansion near the Z^0 resonance,” *Phys. Lett. B* **272** (1991) 353–358. (page 8).
- [48] T. van Ritbergen and R. G. Stuart, “On the precise determination of the Fermi coupling constant from the muon lifetime,” *Nucl. Phys. B* **564** (2000) 343–390 [[hep-ph/9904240](#)]. (pages 5, 8, 10).
- [49] A. J. Buras and P. H. Weisz, “QCD Nonleading Corrections to Weak Decays in Dimensional Regularization and ’t Hooft-Veltman Schemes,” *Nucl. Phys. B* **333** (1990) 66–99. (pages 5, 28).
- [50] G. ’t Hooft and M. J. G. Veltman, “Regularization and Renormalization of Gauge Fields,” *Nucl. Phys. B* **44** (1972) 189–213. (page 6).
- [51] C. G. Bollini and J. J. Giambiagi, “Dimensional Renormalization: The Number of Dimensions as a Regularizing Parameter,” *Nuovo Cim. B* **12** (1972) 20–26.
- [52] P. Breitenlohner and D. Maison, “Dimensional Renormalization and the Action Principle,” *Commun. Math. Phys.* **52** (1977) 11–38. (page 6).
- [53] H. B lusca-Ma ito, A. Ilakovac, M. Ma or-Bo zinovi c, and D. St ckinger, “Dimensional regularization and Breitenlohner-Maison/’t Hooft-Veltman scheme for γ_5 applied to chiral YM theories: full one-loop counterterm and RGE structure,” *JHEP* **08** (2020) 024 [[arXiv:2004.14398](#)]. (page 8).
- [54] T. Kinoshita and A. Sirlin, “Radiative corrections to Fermi interactions,” *Phys. Rev.* **113** (1959) 1652–1660. (page 8).
- [55] Y. Nir, “The Mass Ratio m_c/m_b in Semileptonic b-Decays,” *Phys. Lett. B* **221** (1989) 184–190.
- [56] T. van Ritbergen and R. G. Stuart, “Complete two loop quantum electrodynamic contributions to the muon lifetime in the Fermi model,” *Phys. Rev. Lett.* **82** (1999) 488–491 [[hep-ph/9808283](#)]. (page 9).
- [57] M. Steinhauser and T. Seidensticker, “Second order corrections to the muon lifetime and the semileptonic B decay,” *Phys. Lett. B* **467** (1999) 271–278 [[hep-ph/9909436](#)].
- [58] A. Ferroglia, G. Ossola, and A. Sirlin, “Considerations concerning the radiative corrections to muon decay in the Fermi and standard theories,” *Nucl. Phys. B* **560** (1999) 23–32 [[hep-ph/9905442](#)].
- [59] A. Pak and A. Czarnecki, “Mass effects in muon and semileptonic $b \rightarrow c$ decays,” *Phys. Rev. Lett.* **100** (2008) 241807 [[arXiv:0803.0960](#)].
- [60] M. Fael, K. Sch nwald, and M. Steinhauser, “Third order corrections to the semileptonic $b \rightarrow c$ and the muon decays,” *Phys. Rev. D* **104** (2021) 016003 [[arXiv:2011.13654](#)].
- [61] M. Czakon, A. Czarnecki, and M. Dowling, “Three-loop corrections to the muon and heavy quark decay rates,” *Phys. Rev. D* **103** (2021) L111301 [[arXiv:2104.05804](#)]. (page 8).
- [62] W. J. Marciano and A. Sirlin, “Radiative Corrections to Neutrino Induced Neutral Current Phenomena in the $SU(2)_L \times U(1)$ Theory,” *Phys. Rev. D* **22** (1980) 2695. [Erratum: *Phys.Rev.D* 31, 213 (1985)]. (page 9).
- [63] D. Bigi, M. Bordone, P. Gambino, U. Haisch, and A. Piccione, “QED effects in inclusive semi-leptonic B decays,” *JHEP* **11** (2023) 163 [[arXiv:2309.02849](#)]. [Erratum: *JHEP* 03, 078 (2025)]. (pages 10, 11).

- [64] W. J. Marciano and A. Sirlin, “Radiative corrections to π_{l2} decays,” *Phys. Rev. Lett.* **71** (1993) 3629–3632. (page 11).
- [65] D. Atwood and W. J. Marciano, “Radiative Corrections and Semileptonic B Decays,” *Phys. Rev. D* **41** (1990) 1736. (page 11).
- [66] J. Brod and M. Gorbahn, “Electroweak Corrections to the Charm Quark Contribution to $K^+ \rightarrow \pi^+ \nu \bar{\nu}$,” *Phys. Rev. D* **78** (2008) 034006 [[arXiv:0805.4119](#)]. (page 11).
- [67] M. Gorbahn, S. Jäger, F. Moretti, and E. van der Merwe, “Semileptonic weak Hamiltonian to $\mathcal{O}(\alpha\alpha_s)$ in momentum-space subtraction schemes,” *JHEP* **01** (2023) 159 [[arXiv:2209.05289](#)]. (page 11).
- [68] R. Gatto and M. A. Ruderman, “A suggestion on the theory of the $\pi \rightarrow e + \nu$ to $\pi \rightarrow \mu + \nu$ ratio,” *Nuovo Cim.* **8** (1958) 775–777. (page 12).
- [69] R. Decker and M. Finkemeier, “Short and long distance effects in the decay $\tau \rightarrow \pi \nu_\tau(\gamma)$,” *Nucl. Phys. B* **438** (1995) 17–53 [[hep-ph/9403385](#)].
- [70] T. Kinoshita, “Everyone makes mistakes: Including Feynman,” *J. Phys. G* **29** (2003) 9–22 [[hep-ph/0101197](#)]. (page 12).
- [71] A. Desiderio *et al.*, “First lattice calculation of radiative leptonic decay rates of pseudoscalar mesons,” *Phys. Rev. D* **103** (2021) 014502 [[arXiv:2006.05358](#)]. (page 12).
- [72] D. Giusti, C. F. Kane, C. Lehner, S. Meinel, and A. Soni, “Methods for high-precision determinations of radiative-leptonic decay form factors using lattice QCD,” *Phys. Rev. D* **107** (2023) 074507 [[arXiv:2302.01298](#)].
- [73] R. Frezzotti, *et al.*, “Lattice calculation of the D_s meson radiative form factors over the full kinematical range,” *Phys. Rev. D* **108** (2023) 074505 [[arXiv:2306.05904](#)]. (page 12).
- [74] **BESIII** Collaboration, “Measurement of the absolute branching fractions for purely leptonic D_s^+ decays,” *Phys. Rev. D* **104** (2021) 052009 [[arXiv:2102.11734](#)]. (pages 12, 19).
- [75] **BESIII** Collaboration, “Improved measurement of the branching fraction of $D_s^+ \rightarrow \mu^+ \nu_\mu$,” *Phys. Rev. D* **108** (2023) 112001 [[arXiv:2307.14585](#)]. (page 19).
- [76] **BESIII** Collaboration, “Measurement of the branching fraction of $D_s^+ \rightarrow \ell^+ \nu_\ell$ via $e^+ e^- \rightarrow D_s^{*+} D_s^{*-}$,” *Phys. Rev. D* **110** (2024) 052002 [[arXiv:2407.11727](#)]. (pages 12, 20).
- [77] **BESIII** Collaboration, “Measurement of the Absolute Branching Fraction of $D_s^+ \rightarrow \tau^+ \nu_\tau$ via $\tau^+ \rightarrow e^+ \nu_e \bar{\nu}_\tau$,” *Phys. Rev. Lett.* **127** (2021) 171801 [[arXiv:2106.02218](#)]. (page 20).
- [78] **BESIII** Collaboration, “Measurement of the branching fraction of leptonic decay $D_s^+ \rightarrow \tau^+ \nu_\tau$ via $\tau^+ \rightarrow \pi^+ \pi^0 \bar{\nu}_\tau$,” *Phys. Rev. D* **104** (2021) 032001 [[arXiv:2105.07178](#)].
- [79] **BESIII** Collaboration, “Measurement of the branching fraction of $D_s^+ \rightarrow \tau^+ \nu_\tau$ via $\tau^+ \rightarrow \mu^+ \nu_\mu \bar{\nu}_\tau$,” *JHEP* **09** (2023) 124 [[arXiv:2303.12468](#)].
- [80] **BESIII** Collaboration, “Updated measurement of the branching fraction of $D_s^+ \rightarrow \tau^+ \nu_\tau$ via $\tau^+ \rightarrow \pi^+ \bar{\nu}_\tau$,” *Phys. Rev. D* **108** (2023) 092014 [[arXiv:2303.12600](#)]. (pages 12, 20).
- [81] T. Kinoshita, “Mass singularities of Feynman amplitudes,” *J. Math. Phys.* **3** (1962) 650–677. (page 12).
- [82] G. Feinberg, ed., “Degenerate Systems and Mass Singularities,” *Phys. Rev.* **133** (1964) B1549–B1562. (page 12).

- [83] D. A. Bryman, P. Depommier, and C. Leroy, “ $\pi \rightarrow e\nu$, $\pi \rightarrow e\nu\gamma$ decays and related processes,” *Phys. Rept.* **88** (1982) 151–205. (page 13).
- [84] D. R. Yennie, S. C. Frautschi, and H. Suura, “The infrared divergence phenomena and high-energy processes,” *Annals Phys.* **13** (1961) 379–452. (page 14).
- [85] S. Weinberg, “Infrared photons and gravitons,” *Phys. Rev.* **140** (1965) B516–B524. (page 17).
- [86] G. Isidori, “Soft-photon corrections in multi-body meson decays,” *Eur. Phys. J. C* **53** (2008) 567–571 [[arXiv:0709.2439](#)]. (pages 14, 17, 30).
- [87] T. Kinoshita, “Radiative corrections to $\pi - e$ decay,” *Phys. Rev. Lett.* **2** (1959) 477. (pages 15, 31).
- [88] M. Rowe, *Structure-dependent quantum electrodynamics in heavy meson physics*. PhD thesis, Edinburgh U., 2024. (page 16).
- [89] E. Barberio, B. van Eijk, and Z. Was, “PHOTOS: A Universal Monte Carlo for QED radiative corrections in decays,” *Comput. Phys. Commun.* **66** (1991) 115–128. (page 21).
- [90] E. Barberio and Z. Was, “PHOTOS: A Universal Monte Carlo for QED radiative corrections. Version 2.0,” *Comput. Phys. Commun.* **79** (1994) 291–308.
- [91] P. Golonka and Z. Was, “PHOTOS Monte Carlo: A Precision tool for QED corrections in Z and W decays,” *Eur. Phys. J. C* **45** (2006) 97–107 [[hep-ph/0506026](#)].
- [92] N. Davidson, T. Przedzinski, and Z. Was, “PHOTOS interface in C++: Technical and Physics Documentation,” *Comput. Phys. Commun.* **199** (2016) 86–101 [[arXiv:1011.0937](#)]. (page 21).
- [93] **HPQCD** Collaboration, “ $B \rightarrow K$ and $D \rightarrow K$ form factors from fully relativistic lattice QCD,” *Phys. Rev. D* **107** (2023) 014510 [[arXiv:2207.12468](#)]. (page 24).
- [94] **Fermilab Lattice, MILC** Collaboration, “ D -meson semileptonic decays to pseudoscalars from four-flavor lattice QCD,” *Phys. Rev. D* **107** (2023) 094516 [[arXiv:2212.12648](#)]. (pages 24, 25).
- [95] **ETM** Collaboration, “Scalar and vector form factors of $D \rightarrow \pi(K)\ell\nu$ decays with $N_f = 2 + 1 + 1$ twisted fermions,” *Phys. Rev. D* **96** (2017) 054514 [[arXiv:1706.03017](#)]. [Erratum: *Phys.Rev.D* 99, 099902 (2019), Erratum: *Phys.Rev.D* 100, 079901 (2019)]. (page 26).
- [96] **ETM** Collaboration, “Tensor form factor of $D \rightarrow \pi(K)\ell\nu$ and $D \rightarrow \pi(K)\ell\ell$ decays with $N_f = 2 + 1 + 1$ twisted-mass fermions,” *Phys. Rev. D* **98** (2018) 014516 [[arXiv:1803.04807](#)]. (page 26).
- [97] M. Rowe and R. Zwicky, “Structure-dependent QED in $B^- \rightarrow \ell^- \bar{\nu}(\gamma)$,” *JHEP* **07** (2024) 249 [[arXiv:2404.07648](#)]. (page 27).